Static Calibration of the Tactical Grade Inertial Measurement Units

THESIS

Presented in Partial Fulfillment of the Requirements for the Degree Master of Science in the Graduate School of The Ohio State University

By

Adem Gokhan Hayal

Graduate Program in Geodetic Science and Surveying

The Ohio State University

2010

Master's Examination Committee:

Christopher Jekeli, Advisor

Alan Saalfeld

Abstract

The demand for precise positioning grows up parallel to the advances in production of the geolocation instruments. Today, the Global Positioning System (GPS) is the most common positioning system in use because of its being very precise, convenient and cheap. However, when working in such areas that the external references (e.g. GPS satellites) are not available, a system that does not require information from any external source of information is required. Especially, these kinds of systems necessitate in detection of unexploded ordnances (UXO) buried in forestry areas, where precise position information is vital for removing them. The Inertial Navigation System (INS) operates in any environment and does not depended on any external source of information. It can operate alone or as an integrated system with GPS. However, the Inertial Measurement Unit (IMU) sensor outputs include some errors which can cause very large positioning errors. These errors can significantly be reduced by using calibration methods. The most accurate calibration methods are performed in laboratories and they require very precise instruments. However, the most significant IMU errors, biases and scale factor errors, change from turn on to turn on of the IMU and therefore they need to be estimated before every mission. The Multi-Position Calibration Method developed by Shin (2002) is a good example which is cost efficient and it can be applied in the field without use of any external calibration instrument. The method requires

numerous IMU attitude measurements and use the gravity magnitude and Earth rotation rate as reference for calibration.

The performance of the Multi-Position Calibration Method was tested by using a cart based geolocation system which includes 2 tactical grade IMUs, Honeywell HG1700 and HG1900. The calibration test was conducted in a parking lot of Ohio State University on 06 June 2010. The calibration estimations have shown that the navigation accuracy could be improved by up to 19.8% for the HG1700 and 17.8% for the HG1900. However, the results were not consistent among each other and in some cases decrease in the positioning accuracy was yielded.

Dedication

This document is dedicated to my family.

Acknowledgments

I would like to show my deep gratitude to my academic adviser Dr. Christopher Jekeli for

providing me the opportunity of being one of his graduate students and for his continuous

guidance and encouragements throughout my research. My special appreciations go to

my committee member Dr. Alan Saalfeld for reviewing my thesis and providing his

valuable recommendations. This thesis would not have been possible to complete without

Dr. Jong Ki Lee's technical assistances. I would like to acknowledge my colleagues Sibel

Uzun for helping me with her great adjustment computation skills and Dana Caccamise

for providing me the required instruments for my field test.

Vita

June 1998 ....Trabzon Ataturk High School

June 2000 ....Two-Year Associate's degree in Map and

Cadastre, Karadeniz Technical University

June 2005 ....B.S. Surveying (Geomatics) Engineering,

Karadeniz Technical University

December 2005-March 2007 ....Graduate Research Associate, Department

of Surveying (Geomatics) Engineering,

Karadeniz Technical University

June 2008 to present ....Graduate Research Associate, Department

of Geodetic Science, The Ohio State

University

Fields of Study

Major Field: Geodetic Science and Surveying

Table of Contents

List of Tables

x

List of Figures

Chapter 1: Introduction

"Geolocation, or determining coordinates of points on or above the Earth's surface, is one of the principal tasks in geodesy and has a history of over two thousand years. Modern methods are taking advantage increasingly of satellite-based radar navigation systems, such as the Global Positioning System (GPS), which offer centimeter level precision for static measurements and sub-decimeter precision for mobile systems" (Jekeli and Lee, 2007). However, even though it is currently the most accurate and the only fully operating satellite point positioning system, GPS is not able to work in some situations such as when it loses its connection with the satellites. In addition, GPS positioning accuracy depends on the quality if the information received from the satellites and the atmospheric conditions. Moreover, Nassar and El-Sheimy (2005) note that GPS is not capable of performing some applications that require a very high data rate (e.g. 100-200 Hz). Therefore, the Inertial Navigation System (INS), although it was invented much earlier than GPS, continues to play an important role in positioning and navigation applications because it is independent of any external sources and it provides high frequency data (e.g. 100Hz for HG1700).

INS is a system that basically determines the position by using the rate of rotation and acceleration of the vehicle as indicated by its inertial sensors based on the Newton's laws of motion. Therefore, it is impossible for external sources to interfere with INS, which makes the use of INS important especially in military missions. However, the inertial

sensors in an Inertial Measurement Unit (IMU) contain some deterministic and random errors that have a very strong effect on positioning accuracy, particularly for low-cost IMUs. These errors should be determined and the IMU measurements should be corrected based on the estimated errors. This procedure is called calibration.

IMU Calibration is the process of determining the errors on the gyros and accelerometers and is essential in order to increase the accuracy of INS. In the calibration process, the deterministic errors (biases, scale factor errors and non-orthogonality errors) are estimated by comparing the instrument outputs with known data and the random errors, noise, are minimized by filtering methods.

Various kinds of calibration methods for determining the IMU errors have been developed by scientists. Today, most commonly used calibration methods are using precise laboratory instruments, using data collected in the field by orienting the IMU in different attitudes and using adjustment techniques for determining errors, and/or using different de-noising techniques (filters). Some of the current calibration methods are presented below. The following studies are mostly focused on using low-cost strapdown IMUs.

Aggarwal et al. (2008) use different methods to estimate different error parameters including the use of precise laboratory tools. They first use Allan variance for estimating the noise in the Micro-Electro-Mechanical Systems (MEMS) sensors. Then, by mounting the IMU on a leveled table with each axis of the IMU can precisely be pointed up and down and a precision rate turntable that the unit can be rotated with certain rotation rate, the authors apply a six-position static test and angle rate test for calibration of the

deterministic errors for accelerometer and gyroscope sensors, respectively. Finally, the authors develop an accurate thermal-dependent stochastic model by using a thermal chamber. The authors test their methods by using a GPS/INS integrated system in the field with different scenarios. Their results show that the bias is the most dominant error and the thermal variations also have significant effect on the errors.

However, the study above requires laboratory equipment and cannot be applied during a mission in the field. Use of additional sensors is another solution for IMU calibration. Nebot et al. (1999) performed a study that can be an example for this kind of field calibration procedures. They classify the sensors that are commonly used in navigation applications into two categories: dead-reckoning sensors (internal sensors of an IMU) and external sensors. The authors notice that the dead-reckoning sensors accumulate error over time and these sensors should be reset by using information from external sensors which provide absolute information. Therefore, they used two extra gyros to measure the tilt angles, bank and elevation angles. Then, these additional angular values are used for determining the IMU sensor biases and orientation of the platform on which the unit is mounted. The authors conclude that their method is accurate enough to allow navigation with INS for an extended time with low dead-reckoning IMU sensor errors.

Nevertheless, a calibration procedure that does not require any laboratory instrument and any external device will be more convenient, less costly and, most importantly, can be applied in the field directly.

Shin and El-Sheimy (2002) develop a field calibration method that does not require in-lab calibration procedure, and where the IMU is aligned to the local level frame. The

3

calibration method is developed based on the fact that the IMU sensors measure the Earth

rotation rate and the gravity magnitude independent of the direction where the axes are

pointing. The authors use IMU measurements for different attitudes in which the IMU is

rotated. Then, they estimate the related error parameters by applying the mathematical

method they developed. With the new calibration method, the authors conclude that the

accelerometer bias, scale factor and non-orthogonality errors can be estimated. However,

only gyro biases can realistically be determined because the Earth rotation rate is a very

weak signal and significant parameters are hidden in the noise, which is also addressed

by many authors such as Salychev (1998) and Chatfield (1997). Thus, scale factor and

non-orthogonality errors of gyroscope should be determined by an in-lab calibration

procedure.

Similarly, Shin (2001) uses the same calibration model developed by Shin and El-Sheimy

(2002) in his thesis. Since the Earth rotation rate is a very weak signal and the non-

orthogonalities are hard to determine in the field, Shin only considers bias error for

gyroscopes and bias and scale factor errors for accelerometers. Shin claims that for the

mid-latitude areas, gyroscope calibration can be performed by the measurements where

the IMU is set on a level surface while additional tilting is necessary for accelerometer

calibration in order to avoid singularities in the calculations. Based on the field test

results, Shin concludes that 2-3 minutes of measurements for six or more different

attitudes are enough for gyroscope calibration, but the measurement time should be

increased to 5 minutes for accelerometer calibration in order to reduce almost half of the

positioning error.

Syed et al. (2007) claims that Shin's method has some deficiencies, such as using the Earth rotation rate as a reference for the gyroscope calibration. They also point out that the Earth rotation rate is too weak to be used for this purpose. Therefore, Syed et al. (2007) modify the new calibration method, which is named as multi-position calibration method by the authors, and call it the modified multi-position calibration method. The modification is done by using a single-axis turntable, which does not require special aligned mounting. By producing a high rotation rate as the reference signal instead of the Earth rotation rate, the gyroscope scale factor and non-orthogonality errors are estimated. Moreover, the new multi-positioning method uses the IMU measurements from each IMU axis, pointed approximately up and down, in order to provide approximate initial values for the bias and scale factor error. The field test results show that the new multi-position calibration method can be used instead of the in-lab calibration methods, such as the six-position static test developed by Aggarwal et al. The new method is also less costly (because it requires only a single-axis turntable) and requires less time for calibration.

The previous two studies, Shin and El-Sheimy (2002) and Syed et al. (2007), determine three types of deterministic IMU sensor errors: bias, scale factor and non-orthogonality errors. However, de-noising techniques are also necessary for reducing non-deterministic sensor errors. A good example of this technique is found in Nassar and El-Sheimy (2005).

Nassar and El-Sheimy (2005) apply the wavelet techniques to the IMU sensor measurements and aim to minimize the undesirable effects of sensor noise and other

unspecified high frequency disturbances. The results show that by choice of appropriate level of decomposition (LOD), positioning accuracy improves by 34% - 63% when it is compared to original IMU measurements. The authors claim that the advantage of the wavelet de-noising technique is its being capable of performing local signal analyses. They also point out another advantage of the wavelet technique as its being able to reconstruct the signal from its wavelet coefficients without losing any significant information.

For better inertial sensor error models, in their subsequent work, Nassar and El-Sheimy (2006) use a combined method including autoregressive (AR) process and multi-resolution techniques. The authors prefer the AR process instead of the commonly used Gauss-Markov process, and they use the wavelet multi-resolution technique for improving the quality of IMU data. They apply both of the methods individually and as the combined model to IMU/DGPS data which include Differential GPS (DGPS) signal outages. The results show that the combined algorithm provides better positioning performance by more than 30% compared to when the two methods are applied individually.

In-lab calibration procedure may not be as accurate as field calibration because the inertial sensor errors are changing from switch on to switch on. Therefore, the need for a calibration method that can be applied in real time has become more urgent. The purpose of this study is to perform a field calibration test that can be done in the field and does not require any external instrument in order to improve INS positioning accuracy. For this

purpose, the multi-position calibration method developed by Shin (2001) will be applied on two medium level IMUs: HG1700 and HG1900.

The basics of the Inertial Navigation are described in Chapter 2 while Chapter 3 comprises the calibration methodology with relevant equations and Chapter 4 presents the simulation study with the results. Finally, Chapter 5 comprises the performance analyses of the field calibration test and Chapter 6 includes the conclusions and future suggestions.

Chapter 2: Inertial Navigation

2.1 Coordinate Frames

The coordinate frames used in navigating with IMU are divided into five groups; the inertial frame, the Earth-Centered-Earth-Fixed frame, the navigation frame, the body frame and the sensor frame.

2.1.1 Inertial Frame

The inertial frame, or i-frame, is the most fundamental frame in geodesy. It is such the frame in which Isaac Newton's laws of motion hold, which means that in the system, a body at rest will stay at rest, and similarly a body in a rectilinear motion will preserve its motion if there is no force applied. The frame is attached to the Earth's center and it is in free-fall. The frame is realized by the observed directions of quasars, extremely faraway celestial objects that transmit radio waves and do not indicate any evidence of changing their locations (Jekeli, 2000). The i-frame has its x axis (x^i) pointing towards the mean vernal equinox, where the ecliptic crosses the celestial equator on the celestial sphere, the z axis (z^i) pointing towards the north celestial pole. Finally, the y axis (y^i) completes a right-handed orthogonal coordinate frame (Salychev, 2004).
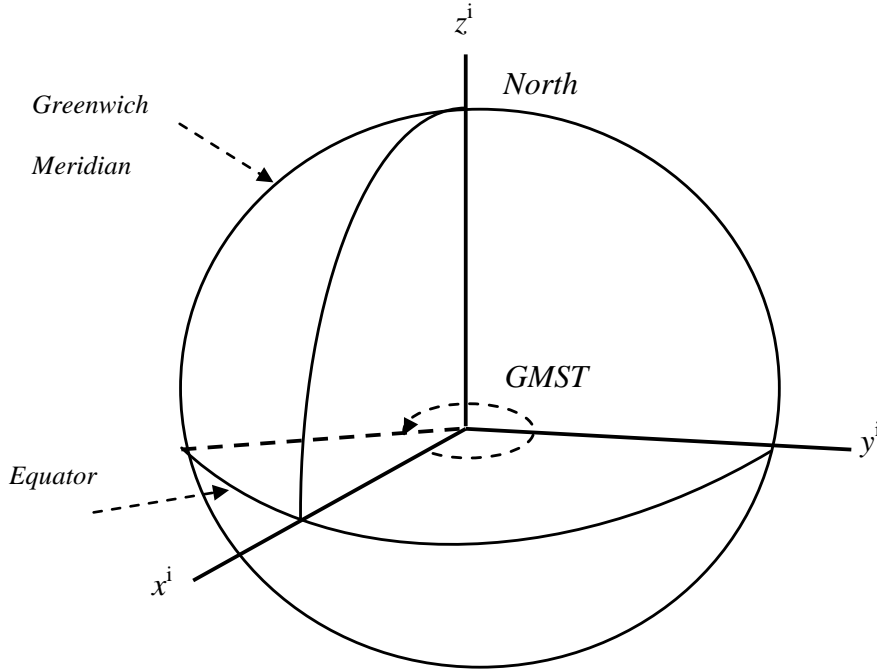
Figure 2.1. The inertial frame

2.1.2 Earth-Centered-Earth-Fixed Frame

The Earth-centered-Earth-fixed frame, or e-frame, is fixed to the Earth and has its origin

at the center of the Earth. Its axes are defined such that the x axis (x^e) is oriented to the

mean Greenwich meridian, the z axis (z^e) is pointing towards the mean polar axis, and the

y axis (y^e) completes a right-handed orthogonal coordinate frame (Jekeli, 2000).

Coordinates of a point in the e-frame can be defined by both the Cartesian coordinates

(x^e, y^e, z^e) and by the ellipsoidal coordinates (φ, λ, h), where φ, λ and h are the geodetic

latitude, the geodetic longitude and the ellipsoidal height (normal distance from the

reference ellipsoid), respectively.
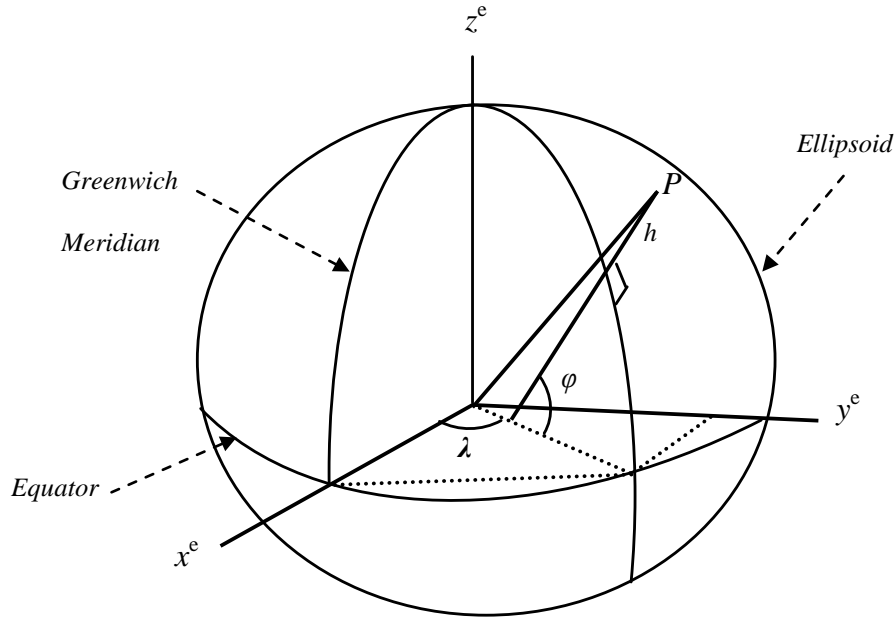
Figure 2.2. The Earth-centered-Earth-fixed frame

2.1.3 Navigation Frame

The navigation frame, or n-frame, is considered as a local coordinate frame moving with

vehicle. It is also known as the local level frame (*l*-frame). The center of the frame is at

the location of the navigation system. The n-frame has its 1-axis pointing north, its 3-axis

pointing downwards and aligned with the ellipsoidal normal, and its 2-axis pointing east

and producing a right-handed Cartesian coordinate frame. Another type of local

coordinate frame available is the north-east-up (NEU) which includes the third axis

pointing up and having positive altitude. However, the NEU frame is a left-handed

coordinate frame and is usually used for astronomic-geodetic observations. The north-

10

east-down (NED) frame is the most commonly used coordinate frame in navigation applications and therefore it is called navigation frame (Jekeli, 2000).
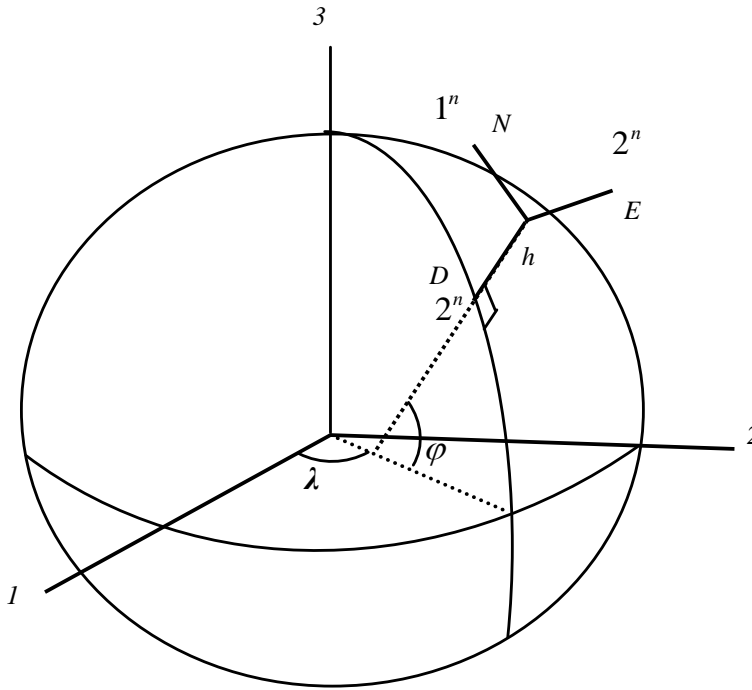
Figure 2.3. The navigation frame (NED)

2.1.4 Body frame

The body frame, or b-frame, is usually associated with the body of the vehicle. The axes of the b-frame are defined such that the x axis (x^b) is pointing towards the front, the y axis (y^b) is pointing towards the right and the z axis (z^b) is pointing downwards, and about which the roll, pitch and yaw angle rotations of the vehicle are defined, respectively.

11
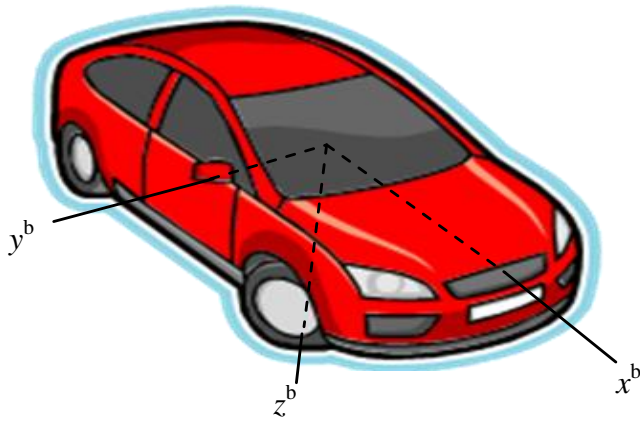
Figure 2.4. The body frame

2.1.5 Instrument Frame

The instrument frame varies based on the manufacturer and the IMU type. Axis
orientation of the Honeywell HG1700 and HG1900 strapdown IMUs is defined by the
manufacturer, Honeywell. The axis x is perpendicular to the top surface and looking up
from the center of the unit, the axis y is orthogonal to the x axis and pointing towards the
connection cable output. The remaining axis z is perpendicular to the other 2 axes and
produces a right-handed orthogonal reference frame.
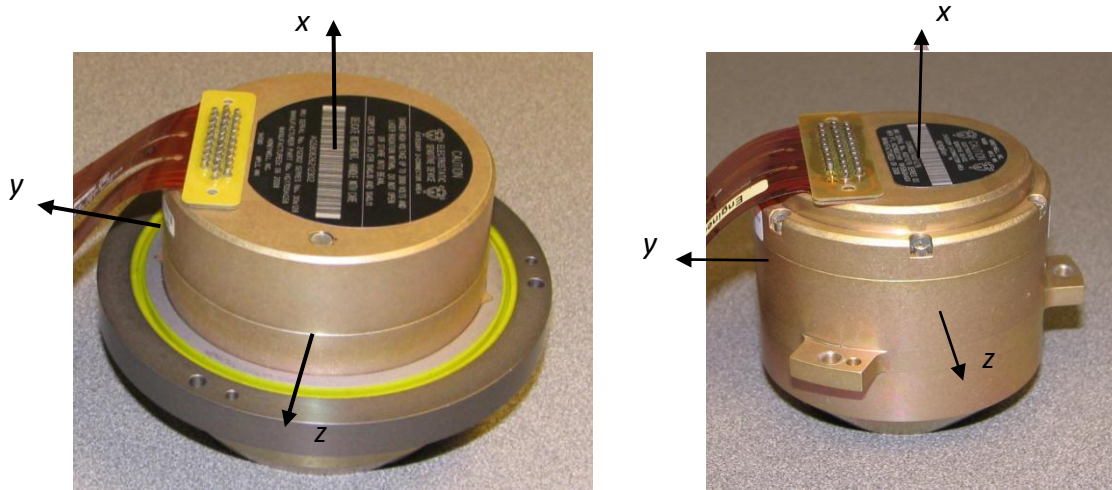
Figure 2.5. The instrument frame, HG1700 (left) and HG1900 (right)

2.2 Inertial Navigation System

INS was invented in the early 20th century and used for marine and land use before and

during World War II. Today, INS is basically used in military applications, such as

missile guidance, space navigation, aviation, marine navigation and especially submarine

navigation, where an external-source-independent navigation system is really necessary.

In general, an INS comprises a computer with adequate hardware and software which

performs the calculations and an IMU with accelerometers, gyroscopes and the platform

on which they are mounted (Jekeli, 2000).

Based on Newton's laws of motion, INS provides position, attitude and orientation of the

vehicle on which the IMU is mounted. Continuously collected acceleration and angular

rate information is required to calculate this navigational information. Therefore, an IMU

includes three accelerometers and three gyroscopes that measure acceleration and angular

rates in the three orthogonal axes: x, y and z axes. The continuous velocity and position information are estimated by successive mathematical integrations of the measured acceleration, and the attitude information is obtained by integration of the measured angular rates. Finally, summing these position and attitude changes with the initial position and heading of the IMU provides the final position of the vehicle.

Two types of INS have been developed; gimbaled INS and strapdown INS (SINS). In the gimbaled INS, the platform where the inertial sensors are mounted is controlled by motorized gimbals so that the platform is always kept aligned with the navigational frame. However, in the strapdown INS the platform is mounted onto the vehicle and kept aligned with the body frame. When it is compared to the strapdown INS, the gimbaled INS is more accurate and requires less computational work, but its bigger size, greater expense and lower operability and also the advances in the mathematical models have caused the strapdown INS to be used more commonly today. Figure 2.6 and 2.7 show the mechanizations of a strapdown INS and a gimbaled INS, respectively.
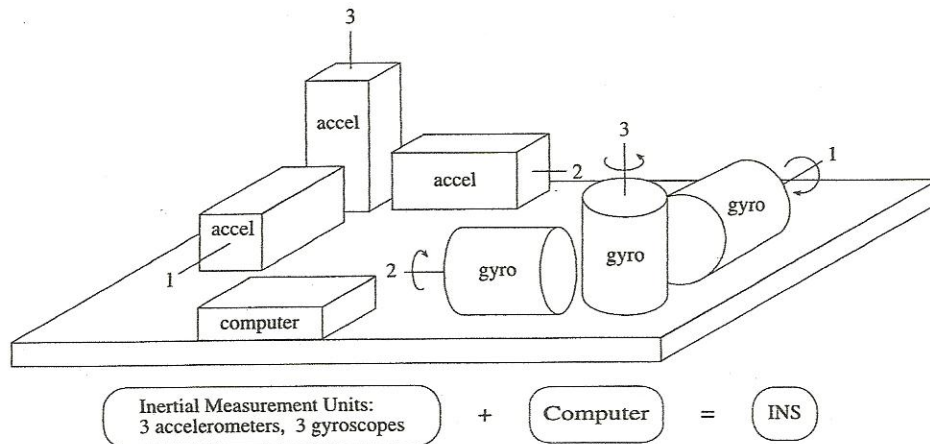
Figure 2.6. Basic Inertial Navigation System (Strapdown INS) comprising IMU's and navigation computer (Jekeli, 2000)
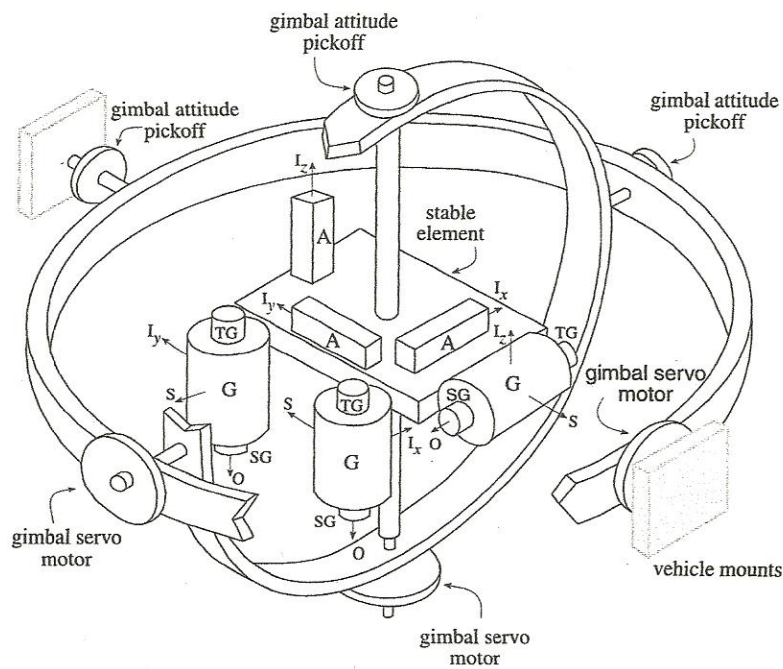
Figure 2.7. Schematic of three-gimbal stabilized platform (G = SDF gyro, A = accelerometer) (Jekeli, 2000)

Based on the error propagation in time, the INS can be categorized as

Low – accuracy: a tactical grade system with accuracy worse than ± 4 km/hr.

Medium – accuracy: a navigation grade system whose accuracy is ± 1-4 km/hr.

High – accuracy: a system with accuracy of ± 0.2 − 1 km/hr, or better (Jekeli, 2000; Yi, 2007).

2.3 IMU Error Sources

Main error sources of the INS are the IMU instrumental errors, the gravity model errors, numerical computation errors, the selected navigation model errors and initialization errors including initial position, velocity and alignment of the IMU. Of these error sources, the IMU instrumental errors are the most significant and dominant ones on navigation accuracy (Yi, 2007).

The IMU consists of accelerometer and gyroscope sensors and the IMU sensor errors are usually divided into 2 parts: deterministic (constant) and non-deterministic (stochastic) errors (Nassar, 2003; Perreault, 2008; Goodall, 2009; etc.). The deterministic errors contain the biases, scale factor errors and non-orthogonality (axes misalignment) errors. The bias is a constant offset and the scale factor error, which is often modeled as constant, creates an error proportional to the magnitude of the IMU measurements. The non-orthogonality error is the misalignment within the IMU axes and has a deterministic and non-deterministic error. Common non-deterministic errors, given by Goodall (2009), are short term instabilities of the sensor errors (noise), angular random walk (ARW),

velocity random walk (VRW), and even bias and scale factor changes due to temperature effects. The difference between the deterministic and non-deterministic errors is; in deterministic errors there needs to be a relationship among observed and output data while the input-output relationship is usually random for the non-deterministic errors. The most common representations of the IMU errors, such as given by Artese and Trecroci (2008), Hou (2004) and Syed et al (2007), are shown below.

The equations for the accelerometer and gyroscope measurements are

$$\underline{Y}_a = \underline{a} + \underline{b}_a + \underline{S}_a \underline{a} + \underline{N}_a \underline{a} + \underline{\eta}_a \qquad (2.1)$$

$$\underline{Y}_\omega = \underline{\omega} + \underline{b}_\omega + \underline{S}_\omega \underline{\omega} + \underline{N}_\omega \underline{\omega} + \underline{\eta}_\omega \qquad (2.2)$$

where $\underline{a}$ is the true specific force vector, $\underline{\omega}$ is the body frame rotation rate vector. Moreover, $\underline{b}$ is the bias vector, $\underline{S}$ is the scale factor error matrix, $\underline{N}$ is the non-orthogonality error matrix, and $\underline{\eta}$ is the noise term including non-deterministic accelerometer errors with the subscripts a and ω representing the accelerometer and gyroscope.

The following table shows factory defined error parameters for the tactical grade IMUs Honeywell HG1700 and HG1900.

Parameter	Units	HG1700	HG1900
Volume	in^3	33	17
Weight	lbs	< 2	< 1
Power	Watts	< 8	< 2
Non-Operating Shock	g max	< 500	< 500
Gyro Performance			
Parameter	Units	HG1700	HG1900
Operating Range	^{o}/sec	± 1074	± 1000
Scale Factor Repeatability	PPM (1σ)	150	150
Scale Factor Linearity	PPM (1σ)	150	150
Bias Repeatability	^{o}/hr (1σ)	1	< 17
Bias (In Run Stability)	^{o}/hr (1σ)	1	< 7
Bias Static g Sensitivity	^{o}/hr/g (1σ)		3
Bias g2 Sensitivity	^{o}/hr/g2 (1σ)		0.6
Bias Acoustic Rectification Error (ARE)	^{o}/hr max		10
Quantization			
Angular Random Walk (ARW)	deg/√hr max	0.125	0.09
Axis Alignment Stability	µ rad (1σ)	500	80
Axis Alignment Stability (non-orthogonality)	µ rad (1σ)	100	50
Accelerometer Performance			
Parameter	Units	HG1700	HG1900
Operating Range	g	70	70
Scale Factor Error	PPM (1σ)	300	300
Scale Factor Linearity	PPM (1σ)	500	500
Bias Repeatability	m-g (1σ)	1	1
Bias Stability	m-g (1σ)	1	1
Vibration Shift	µ-g max	500	500
Axis Alignment Stability (non-orthogonality)	µ rad (1σ)	100	100
Velocity Random Walk (VRW)	(m/s) /√hr max	0.22	0.22

Table 2.1. Tactical comparison of HG1700 and HG1900 (Honeywell Tactical Inertial Measurement Units (IMU), 2007)

2.4 Calibration Methods

Based on the required equipment and error estimation procedures, the IMU calibration methods can be classified in 3 sections: laboratory calibration methods (Section 2.4.1) and field calibration methods (Section 2.4.2) for calibration of the deterministic IMU errors and stochastic models (Section 2.4.3) for the non-deterministic IMU errors.

2.4.1 Laboratory Calibration Methods

These methods require the use of precise instruments for orienting the IMU to certain

directions, or rotating the IMU in desired directions with desired rotation rates. Usually

these calibration instruments are costly.

In their study, Aggarwal et al. (2008) provide detailed analyses of the laboratory

calibration methods under the following titles and as explained below.

2.4.1.1 Six-Position Static Test

Aggarwal et al. (2008) state that an error calibration model can be established by

mounting the IMU on a leveled turntable and aligning the IMU axes alternately up and

down with respect to different angle rotations. Then ignoring the remaining error sources

given in (2.1) and (2.2), the bias (b) and scale factor error (S) are estimated via the

following equations by the authors. The up and down oriented sensor measurements of an

IMU axis will be

$$Y^{up} = b + (1+S)K \tag{2.3}$$

$$Y^{down} = b - (1+S)K \tag{2.4}$$

where Y^{up} and Y^{down} are the sensor measurements when the related IMU axis is pointing

alternately upward and downward. K is the corresponding component of the Earth

rotation rate for gyroscope and the gravity magnitude for accelerometer measurements.

Then, the bias and scale factor error are estimated as follows

$$b = (Y^{up} + Y^{down})/2 \tag{2.5}$$

$$S = (Y^{up} - Y^{down} - 2K)/2K \tag{2.6}$$

The procedure is repeated for each IMU axis sequentially and biases and scale factor

errors are estimated.

However, Aggarwal et al. (2008) and Syed et al. (2007) claim that accuracy of this six-

position static test, the method described above, depends on the how well the IMU is

aligned with the vertical axes of the local level frame and it is only possible to calculate

the biases and scale factor errors with this standard method. In order to be able to

estimate the non-orthogonality errors, the authors modify the above method and call it the

improved six-position test. The modified method is explained below.

In case of accelerometers, by ignoring $\underline{S}_{2a}$, $\underline{\eta}_a$ and $\underline{\delta}_g$ in 2.1, the IMU attitude

measurements are shown as below.

$$\underline{Y}_a = \underline{a} + \underline{b}_a + \underline{S}_a \underline{a} + \underline{N}_a \underline{a} \tag{2.7}$$

Then, the authors represent the measured accelerometer values for one IMU attitude by

the following matrix form.

$$\begin{bmatrix} Y_{ax} \\ Y_{ay} \\ Y_{az} \end{bmatrix} = \begin{bmatrix} m_{axx} & m_{axy} & m_{axz} \\ m_{ayx} & m_{ayy} & m_{ayz} \\ m_{azx} & m_{azy} & m_{azz} \end{bmatrix} \begin{bmatrix} a_x \\ a_y \\ a_z \end{bmatrix} + \begin{bmatrix} b_{ax} \\ b_{ay} \\ b_{az} \end{bmatrix}, \text{ or}$$

$$
\underbrace{\begin{bmatrix} Y_{ax} \\ Y_{ay} \\ Y_{az} \end{bmatrix}}_{\underline{Y}_{a1}} = \underbrace{\begin{bmatrix} m_{axx} & m_{axy} & m_{axz} & b_{ax} \\ m_{ayx} & m_{ayy} & m_{ayz} & b_{ay} \\ m_{azx} & m_{azy} & m_{azz} & b_{az} \end{bmatrix}}_{\underline{X}} \underbrace{\begin{bmatrix} a_x \\ a_y \\ a_z \\ 1 \end{bmatrix}}_{\underline{A}_{a1}}
\tag{2.8}
$$

The diagonal m elements in $\underline{X}$ represent the scale factor errors (m_{ii}), the remaining m elements (m_{ij}) denote the non-orthogonality errors while b_{ai} and a_i symbolize the accelerometer bias and true accelerations, respectively (where i, j: x, y and z). Then, by perfectly aligning the IMU axes up and down as in the standard six-position test, the true accelerations will be

$$
\underline{A}_{a1}^{x-up} = \begin{bmatrix} g \\ 0 \\ 0 \end{bmatrix}, \underline{A}_{a2}^{x-down} = \begin{bmatrix} -g \\ 0 \\ 0 \end{bmatrix}, \underline{A}_{a3}^{y-up} = \begin{bmatrix} 0 \\ g \\ 0 \end{bmatrix},
$$

$$
\tag{2.9}
$$

$$
\underline{A}_{a4}^{y-down} = \begin{bmatrix} 0 \\ -g \\ 0 \end{bmatrix}, \underline{A}_{a5}^{z-up} = \begin{bmatrix} 0 \\ 0 \\ g \end{bmatrix}, \underline{A}_{a6}^{z-down} = \begin{bmatrix} 0 \\ 0 \\ -g \end{bmatrix}
$$

where g is the mean gravity magnitude for the point the IMU is placed, the subscripts ai represent the IMU attitude numbers ($1 < i < 6$) and superscripts denote the up and down orientations of the related IMU axes.

The matrix of observed accelerations is produced as

$$\underline{Y}_a = \begin{bmatrix} \underline{Y}_{a1}^{x-up} & \underline{Y}_{a2}^{x-down} & \underline{Y}_{a3}^{y-up} & \underline{Y}_{a4}^{y-down} & \underline{Y}_{a5}^{z-up} & \underline{Y}_{a6}^{z-down} \end{bmatrix}_{3\times6} \tag{2.10}$$

The Least Squares Solution is used for calculating the desired error parameters, the matrix X.

$$\underset{[3\times4]}{\underline{X}} = \underset{[3\times6]}{\underline{Y}}\,\underset{[4\times6]}{\underline{A}^{T}}\,(\underset{[4\times4]}{\underline{AA}^{T}})^{-1} \tag{2.11}$$

where the coefficient matrix of the least squares solution is designed as

$$\underline{A}_a = \begin{bmatrix} \underline{A}_{a1}^{x-up} & \underline{A}_{a2}^{x-down} & \underline{A}_{a3}^{y-up} & \underline{A}_{a4}^{y-down} & \underline{A}_{a5}^{z-up} & \underline{A}_{a6}^{z-down} \\ 1 & 1 & 1 & 1 & 1 & 1 \end{bmatrix}_{4\times6} \tag{2.12}$$

By replacing the gravity components with the Earth rotation rate components, the same model is used for calibration of gyroscopes. Nevertheless, Aggarwal et al. (2008) claim that the six-axis calibration method can only be used for tactical grade or higher grade gyroscopes because of the bias instability and high level noise which masks the Earth rotation rate. Therefore, the rotation rate test is preferred for calibration of the gyroscopes.

2.4.1.2 Rotation Rate Test

The rotation rate test is done by mounting the IMU on a precise rotation table, which is controlled by a computer, and rotating the unit with precisely known angular rates. Usually clockwise and counterclockwise rotations are applied. The same procedure as the

previous method is used for this test as well (Aggarwal et al., 2008). Estimation of the

deterministic IMU errors is done by replacing the up and down gyro measurements (Y^{up}

and Y^{down}) with clockwise and counterclockwise gyro measurements ($Y^{clockwise}$ and

$Y^{counterclockwise}$) together with replacing the reference Earth rotation rate (ω_e) with the

generated rotation rate (ω).

2.4.1.3 Thermal Test

For the low-cost IMU sensors, the errors are very much affected by the changes in the

environmental conditions, especially the temperature. This indicates that the bias and

scale factor error values will be different in the laboratory and in the field. Therefore, a

reliable thermal calibration model is necessary (Aggarwal et al., 2008). Two types of

thermal method are defined by Aggarwal et al. (2008).

In the Soak method, the IMU is put inside of a thermal chamber and the IMU data are

recorded at certain desired temperatures. Then, a linear interpolation technique is used to

produce a model for intermediate temperatures. In the Thermal Ramp method, however,

the temperature is linearly increased or decreased during the data recording for a desired

time interval.

2.4.2 Field Calibration Methods

The previous calibration methods require a laboratory environment and special

instruments. Even though they provide very accurate estimations of the IMU sensor

errors, they are costly. More importantly some of the deterministic errors (biases and

scale factor errors) change from turn-on to turn-on and they need to be estimated before

and/or after every operation in the field.

2.4.2.1 Multi-Position Calibration Method

To fulfill the requirements mentioned above, Shin and El-Sheimy (2002) develop a new

calibration method that does not require any additional equipment other than the IMU

itself. Moreover, special alignment of the IMU is not necessary. By recording the IMU

data with different attitudes, the deterministic sensor errors are estimated. The calibration

method is later named as the multi-position calibration method by Syed et al. (2007). The

method is explained in Section 3 in detail.

2.4.2.2 Modified Multi-Position Calibration Method

However, Syed et al. (2007) noticed that the multi-position calibration method cannot

estimate the gyroscope scale factor and non-orthogonality errors. The authors also claim

that for the low level IMU sensors, it is difficult to converge to reasonable bias and scale

factor error values without having initial values in the adjustment computations. They

resolve these deficiencies of the multi-position calibration method by making 2

modifications on it and call it the modified multi-position calibration method.

First, they include a single axis turntable into the calibration system. The IMU is mounted

on the turntable; then, the gyroscope data are recorded while the turntable is rotating with

a certain rate (however, how they determined the rotation rate was not mentioned in their

study). Then, the desired IMU attitude measurements are done through clockwise and

counterclockwise rotations. The possible attitudes are explained in Section 3.5. In the

modified method, the rotation rate produced by the turntable is used as reference for the

gyroscope calibration instead of using the Earth rotation rate which is a weak signal.

The second modification is done by performing a test similar to the six-position static

test. The IMU axes are approximately oriented up and down directions and rough

estimates of the bias and scale factor are obtained by (2.5) and (2.6), respectively. The

reason that the estimated values are called rough is in this method the IMU orientations

are done approximately while the traditional six-position static test requires perfect

alignments of the IMU axes with the vertical gravity vector. Then, the IMU data are

calibrated for these initially estimated error parameters and the multi-position calibration

method equations are used for calibrating the remaining errors in the IMU data. They,

moreover, state that pre-calibrating the IMU errors improves converging speed in the

adjustment iterations.

2.4.3 Stochastic Models

The estimates of deterministic errors can be improved by using appropriate stochastic

models for the non-deterministic errors, simply noise in the data. These models could be

derived from the studies of the Allan Variance (Aggarwal et al., 2008) and the wavelet

de-noising (Nassar and El-Sheimy, 2005) techniques. The Allan variance is a time

domain analysis technique and it is used for analyzing the characteristics of the random

processes, for example, the noise in the data (Aggarwal et al., 2008).

Nassar and El-Sheimy (2005) note that the noise in the IMU data contains two parts, the

low-frequency (long-term) and high-frequency (short-term) components. The white noise

is included in the high-frequency components while the low frequency components

contain the correlated noise. The correlated noise can be modeled using random processes, and the white noise could be removed using de-noising techniques. Because the main purpose is to analyze the performance of the field calibration method, none of the stochastic models described above were tested in this study.

Chapter 3: Calibration Procedure

An efficient and cost effective INS calibration method was aimed to be analyzed in this

study. The new calibration method, Multi-Position Calibration Method (MPCM), that

was developed by Shin and El-Sheimy (2002) is a good example for this purpose. The

main advantage of this method is it can be applied in the field and does not require any

additional instrument to align the IMU to any certain directions. Therefore, it can be

applied in the field directly and at any time during the operation in order to estimate the

IMU systematic errors, the bias, scale factor and non-orthogonality errors. Moreover,

because the bias and scale factor errors change whenever the IMU is turned on and off,

the necessity of such a calibration method becomes more important.

The calibration procedure is explained in the sections below with related definitions and

calculation steps.

3.1 The Multi-Position Calibration Method

The new method is based on the fact that in the stationary mode, the total magnitude that

the gyroscopes and the accelerometers sense will be the Earth rotation rate and the

gravity magnitude, respectively, independent of the direction that the individual axes are

pointing. By performing an adequate number of IMU measurements at different attitudes

(see Section 3.5 for the possible attitudes) and using the related adjustment technique

mentioned in Section 3.4, the IMU sensor errors are estimated.

3.2 Calibration Model

The calibration model is described by Shin and el Sheimy (2002) as follows.

The following 3 unit vectors are used in order to define a vector in R^3 space in the sensor frame.

$$\underline{x}:(1,\ 0,\ 0),\ \underline{y}:(0,\ 1,\ 0),\ \underline{z}=(0,\ 0,\ 1) \tag{3.1}$$

In case of perfect orthogonality, the sensed values for the accelerometers on each axis with respect to the NED navigation frame can be explained as follows

$$a_x = <-\underline{g}, \underline{x}> = -g \cos \alpha$$

$$a_y = <-\underline{g}, \underline{y}> = -g \cos \beta \tag{3.2}$$

$$a_z = <-\underline{g}, \underline{z}> = -g \cos \gamma$$

where "<-,->" is the inner product, $\underline{g} = \begin{bmatrix} g_x & g_y & g_z \end{bmatrix}^T$ is the gravity vector and α, β, γ are the angles (Figure 3.1) between the local gravity vector and the x, y and z axes of the IMU, respectively.
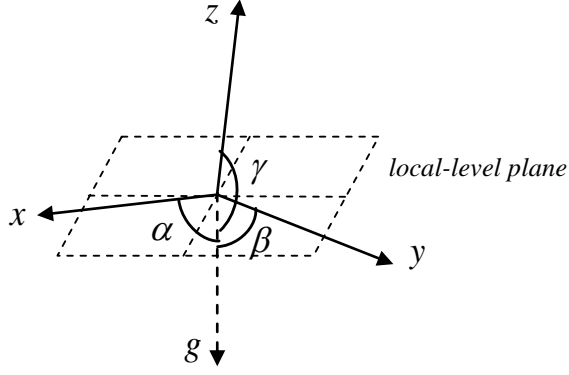
Figure 3.1. Misalignment to n-frame (Shin and El-Sheimy, 2002)

Shin and El-Sheimy (2002) introduce the general calibration model as below and state that it holds regardless of the alignment to the n-frame.

$$a_x^2 + a_y^2 + a_z^2 = \|g\|^2 \left(\cos^2 \alpha + \cos^2 \beta + \cos^2 \gamma \right) = \|g\|^2 \qquad (3.3)$$

By using the same methodology, we can derive the general model for the gyros as

$$\omega_x^2 + \omega_y^2 + \omega_z^2 = \|\omega_e\|^2 \qquad (3.4)$$

where ω_e is the true Earth rotation rate.

However, the IMU axes may not be perfectly orthogonal to each other and the non-orthogonalities among the IMU axes might have significant effects on navigation

accuracy. The non-orthogonality error is an angle that we need to rotate the IMU axes in order to obtain perfect orthogonality.

Shin and El-Sheimy (2002) describe the non-orthogonalities as follows. In order to eliminate the non-orthogonality between the axes x and y, the y axis is rotated about the z axis by the angle θ_{yz} (figure 3.2). This rotation can be shown by the vector below.

$$\underline{y}_1 = \underline{R}_z \, \underline{y} = \begin{bmatrix} -\sin\theta_{yz} & \cos\theta_{yz} & 0 \end{bmatrix}^T, \tag{3.5}$$

where

$$\underline{R}_z = \begin{bmatrix} \cos\theta_{yz} & -\sin\theta_{yz} & 0 \\ \sin\theta_{yz} & \cos\theta_{yz} & 0 \\ 0 & 0 & 1 \end{bmatrix} \tag{3.6}$$

The non-orthogonality of the z axis can be expressed by two consecutive rotations; rotation about the x axis by θ_{zx} and about the y axis by θ_{zy} (figure 3.2).

$$\underline{z}_1 = \underline{R}_x \underline{R}_y \, \underline{z} = \begin{bmatrix} -\sin\theta_{zy} & -\sin\theta_{zx}\cos\theta_{zy} & \cos\theta_{zx}\cos\theta_{zy} \end{bmatrix}^T, \tag{3.7}$$

where

$$\underline{R}_x = \begin{bmatrix} 1 & 0 & 0 \\ 0 & \cos\theta_{zx} & -\sin\theta_{zx} \\ 0 & \sin\theta_{zx} & \cos\theta_{zx} \end{bmatrix}, \text{ and } \underline{R}_y = \begin{bmatrix} \cos\theta_{zy} & 0 & \sin\theta_{zy} \\ 0 & 1 & 0 \\ -\sin\theta_{zy} & 0 & \cos\theta_{zy} \end{bmatrix} \qquad (3.8)$$
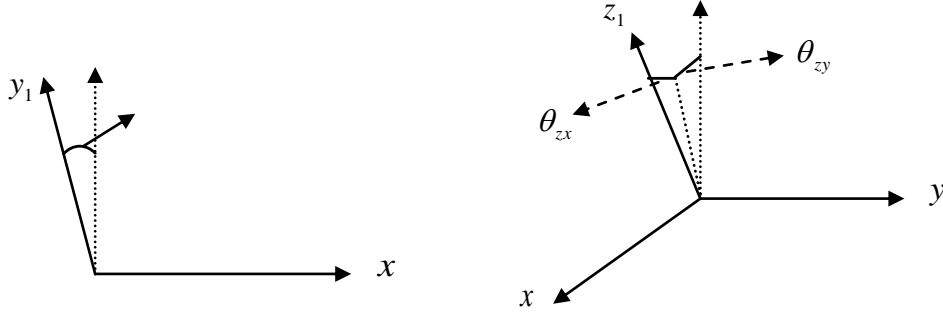
Figure 3.2. Non-orthogonality between y axis and x axis (left), non-orthogonality of z axis to xy plane (right) (Shin and El-Sheimy, 2002)

Finally, the non-orthogonal IMU axes in local level frame can be represented by the vectors below,

$$\underline{x}_1 = \begin{bmatrix} 1 & 0 & 0 \end{bmatrix}^T$$

$$\underline{y}_1 = \begin{bmatrix} -\sin\theta_{yz} & \cos\theta_{yz} & 0 \end{bmatrix}^T \qquad (3.9)$$

$$\underline{z}_1 = \begin{bmatrix} -\sin\theta_{zy} & -\sin\theta_{zx}\cos\theta_{zy} & \cos\theta_{zx}\cos\theta_{zy} \end{bmatrix}^T$$

31

The non-orthogonality angles are quite small, e.g. the manufacturer states standard deviations of 100 μrad for HG1700 and HG1900 (see Table 2.1), and therefore the above vectors can be represented with small angle approximations as below.

$$\underline{x}_1 = \begin{bmatrix} 1 & 0 & 0 \end{bmatrix}^T$$

$$\underline{y}_1 = \begin{bmatrix} -\theta_{yz} & 1 & 0 \end{bmatrix}^T \tag{3.10}$$

$$\underline{z}_1 = \begin{bmatrix} -\theta_{zy} & -\theta_{zx} & 1 \end{bmatrix}^T$$

The accelerometers on the IMU axes sense the following values.

$$a_{x1} = <\underline{a}, \underline{x}_1> = a_x$$

$$a_{y1} = <\underline{a}, \underline{y}_1> = -a_x \sin\theta_{ayz} + a_y \cos\theta_{ayz} \tag{3.11}$$

$$a_{z1} = <\underline{a}, \underline{z}_1> = a_x \sin\theta_{azy} - a_y \sin\theta_{azx} \cos\theta_{azy} + a_z \cos\theta_{azx} \cos\theta_{azy}$$

Inclusion of the major errors, bias and scale factor error, into the IMU data is done by the equation below.

$$Y_{ai} = b_{ai} + (1 + s_{ai})a_i \tag{3.12}$$

where Y_a, b_a, s_a are IMU observation, bias and scale factor error, respectively, for the

accelerometer and a_i is the specific force vector component with $i = $ x, y and z.

After including the non-orthogonalities, the observation equations for the accelerometer

sensors on the IMU axis triad will be obtained as below.

$$Y_{ax} = b_{ax} + (1 + s_{ax})a_x + \eta_{ax}$$

$$Y_{ay} = b_{ay} + (1 + s_{ay})(-a_x \sin\theta_{ayz} + a_y \cos\theta_{ayz}) + \eta_{ay} \qquad (3.13)$$

$$Y_{az} = b_{az} + (1 + s_{az})\begin{pmatrix} a_x \sin\theta_{azy} - a_y \sin\theta_{azx}\cos\theta_{azy} \\ + a_z \cos\theta_{azx}\cos\theta_{azy} \end{pmatrix} + \eta_{az}$$

where η_{ai} is the random sensor noise in the accelerometer measurements ($i = $ x, y and z).

By rearranging the above equations and ignoring the noise terms, the true values for the

specific force vector components are found as

$$a_x = \frac{Y_{ax} - b_{ax}}{1 + s_{ax}}$$

$$a_y = a_x \tan\theta_{ayz} + \frac{Y_{ay} - b_{ay}}{(1 + s_{ay})\cos\theta_{ayz}} \qquad (3.14)$$

$$a_z = -a_x \frac{\tan\theta_{azy}}{\cos\theta_{azx}} + a_y \tan\theta_{azx} + \left(\frac{Y_{az} - b_{az}}{(1 + s_{az})\cos\theta_{azx}\cos\theta_{azy}} \right)$$

We can present the equations 3.13 with the small-angle approximations, which is also shown by Syed et al. (2007) in a matrix form, as follows

$$
\begin{bmatrix} Y_{ax} \\ Y_{ay} \\ Y_{az} \end{bmatrix} = \begin{bmatrix} b_{ax} \\ b_{ay} \\ b_{az} \end{bmatrix} + \begin{bmatrix} 1+s_{ax} & 0 & 0 \\ -\theta_{ayz} & 1+s_{ay} & 0 \\ \theta_{azy} & \theta_{azx} & 1+s_{az} \end{bmatrix} \begin{bmatrix} a_x \\ a_y \\ a_z \end{bmatrix} \tag{3.15}
$$

and the true specific force vector components will be

$$
\begin{aligned}
a_x &= \frac{Y_{ax} - b_{ax}}{1+s_{ax}} \\
a_y &= a_x \theta_{ayz} + \frac{Y_{ay} - b_{ay}}{1+s_{ay}}, \\
a_z &= -a_x \theta_{azy} + a_y \theta_{azx} + \frac{Y_{az} - b_{az}}{1+s_{az}}
\end{aligned} \tag{3.16}
$$

However, due to the advances in the modern computational technologies, there is no need to use the small-angle approximations. Thus, they were not used in this study. The gyroscope observation equations can be produced by replacing specific force vector components (a) with the Earth rotation rate vector components (ω).

$$Y_{\omega x} = b_{\omega x} + \left(1 + s_{\omega x}\right)\omega_x + \eta_{\omega x}$$

$$Y_{\omega y} = b_{\omega y} + \left(1 + s_{\omega y}\right)\left(-\omega_x \sin\theta_{\omega yz} + \omega_y \cos\theta_{\omega yz}\right) + \eta_{\omega y} \qquad (3.17)$$

$$Y_{\omega z} = b_{\omega z} + \left(1 + s_{\omega z}\right)\left(\begin{array}{c} \omega_x \sin\theta_{\omega zy} - \omega_y \sin\theta_{\omega zx}\cos\theta_{\omega zy} \\ + \omega_z \cos\theta_{\omega zx}\cos\theta_{\omega gz} \end{array}\right) + \eta_{\omega z}$$

where $\eta_{\omega i}$ is the random sensor noise for gyroscope (i = x, y and z). The Earth rotation

rate components are then solved:

$$\omega_x = \frac{Y_{\omega x} - b_{\omega x}}{(1 + s_{\omega x})}$$

$$\omega_y = \omega_x \cos\theta_{\omega yz} + \frac{Y_{\omega y} - b_{\omega y}}{(1 + s_{\omega y})\cos\theta_{\omega yz}} \qquad (3.18)$$

$$\omega_z = -\frac{\omega_x}{\cos\theta_{\omega zx}} + \omega_y \tan\theta_{\omega zx} + \left(\frac{Y_{\omega z} - b_{\omega z}}{(1 + s_{\omega z})\cos\theta_{\omega zx}\cos\theta_{\omega zy}}\right)$$

3.3 Generation of the Calibration Model

By using the equations (3.3) and (3.4), Shin and El-Sheimy (2002) produce the

calibration models for gyroscope and accelerometer errors are as follows,

$$f_a = a_x^2 + a_y^2 + a_z^2 - \|g\|^2 = 0 \qquad (3.19)$$

$$f_\omega = \omega_x^2 + \omega_y^2 + \omega_z^2 - \|\omega_e\|^2 = 0 \qquad (3.20)$$

Substituting the equations (3.13) and (3.16) into the calibration model equations, we obtain the calibration model that includes all 9 error parameters as

$$
\begin{aligned}
f_a =& \left(\frac{Y_{gx} - b_{gx}}{1 + s_{gx}} \right)^2 + \left(\tan\theta_{gyz} \frac{Y_{gx} - b_{gx}}{1 + s_{gx}} + \frac{1}{\cos\theta_{gyz}} \frac{Y_{gy} - b_{gy}}{1 + s_{gy}} \right)^2 \\
&+ \left(\begin{aligned} &\left(\tan\theta_{gzx} \tan\theta_{gyz} - \frac{\tan\theta_{gzy}}{\tan\theta_{gzx}} \right) \left(\frac{Y_{gx} - b_{gx}}{1 + s_{gx}} \right) \\ &+ \frac{\tan\theta_{gzx}}{\tan\theta_{gyz}} \left(\frac{Y_{gy} - b_{gy}}{1 + s_{gy}} \right) + \frac{1}{\cos\theta_{gzx} \cos\theta_{gzy}} \left(\frac{Y_{gz} - b_{gz}}{1 + s_{gz}} \right) \end{aligned} \right)^2 \\
&- \|g\|^2 = 0
\end{aligned}
\tag{3.21}
$$

and,

$$
\begin{aligned}
f_\omega =& \left(\frac{Y_{\omega x} - b_{\omega x}}{1 + s_{\omega x}} \right)^2 + \left(\tan\theta_{\omega yz} \frac{Y_{\omega x} - b_{\omega x}}{1 + s_{\omega x}} + \frac{1}{\cos\theta_{\omega yz}} \frac{Y_{\omega y} - b_{\omega y}}{1 + s_{\omega y}} \right)^2 \\
&+ \left(\begin{aligned} &\left(\tan\theta_{\omega zx} \tan\theta_{\omega yz} - \frac{\tan\theta_{\omega zy}}{\tan\theta_{\omega zx}} \right) \left(\frac{Y_{\omega x} - b_{\omega x}}{1 + s_{\omega x}} \right) \\ &+ \frac{\tan\theta_{\omega zx}}{\tan\theta_{\omega yz}} \left(\frac{Y_{\omega y} - b_{\omega y}}{1 + s_{\omega y}} \right) + \frac{1}{\cos\theta_{\omega zx} \cos\theta_{\omega zy}} \left(\frac{Y_{\omega z} - b_{\omega z}}{1 + s_{\omega z}} \right) \end{aligned} \right)^2 \\
&- \|\omega_e\|^2 = 0
\end{aligned}
\tag{3.22}
$$

In case we want to estimate only the bias and scale factor errors, for example we don't have enough observations, the calibration models that comprise only the bias and scale factor solution can be formed as below.

$$f_a = \left(\frac{Y_{ax} - b_{ax}}{1 + s_{ax}} \right)^2 + \left(\frac{Y_{ay} - b_{ay}}{1 + s_{ay}} \right)^2 + \left(\frac{Y_{az} - b_{az}}{1 + s_{az}} \right)^2 - \|g\|^2 = 0 \qquad (3.23)$$

Similarly, the model for solving the bias only is

$$f_a = \left(Y_{ax} - b_{ax} \right)^2 + \left(Y_{ay} - b_{ay} \right)^2 + \left(Y_{az} - b_{az} \right)^2 - \|g\|^2 = 0 \qquad (3.24)$$

By, again, replacing acceleration vector components (a) with the rotation rate vector components (ω) in equations 3.23 and 3.24 we obtain the calibration models for the gyroscope measurements.

3.4 Adjustment Computations

To be able to estimate the gyroscope and accelerometer errors of the IMU, the Least Squares adjustment is used for the calibration models given in the section above. Shin and El- Sheimy (2002) and Syed et al. (2007) used the combined case least square solution with weighted parameters. This method will be called the Gauss-Helmert model in this study. The Gauss-Helmert model requires numerous iterations defined below; however, the iteration steps were not explained in any of those studies above.

Pope (1972) asserts that the Newton-Gauss iteration is usually done incorrectly and explains the correct way in his study. The adjustment procedure that was described by Pope (1972) and summarized by May (2008) is shown below.

The calibration model is

$$f(\underbrace{Y_{obs} - e}_{[3n\times1]}, \underset{[m\times1]}{\Xi}) = \underset{[n\times1]}{0}, \quad e \sim (0, \sigma_0^2 \underset{[3n\times3n]}{P^{-1}}) \tag{3.25}$$

where $f : R^{3n+m} \to R^n$ denotes a given multivariate nonlinear function (Schaffrin and

Snow, 2009) and n is the number of the different attitudes of the IMU (for either

accelerometer or gyroscope measurements) that are used in the calibration, m is the

number of unknown parameters and P is the $3n \times 3n$ weight matrix for the observations.

Moreover, Ξ, e and σ_0^2 represent the unknown parameter vector, the random error vector

and, the variance of unit weight, respectively.

If it was not given, P can be obtained as follows

$$P = \begin{bmatrix} 1/\sigma^2 & 0 & \cdots & 0 \\ 0 & 1/\sigma^2 & & 0 \\ \vdots & & \ddots & \vdots \\ 0 & 0 & \cdots & 1/\sigma^2 \end{bmatrix}_{3n\times3n}, \text{ or } P = (1/\sigma^2) I_{3n\times3n} \tag{3.26}$$

where σ^2 is assumed to be same for each attitude.

Standard deviation of the IMU measurements, σ, can be calculated for accelerometer and

gyroscope measurements from given velocity and angular random walk parameters,

respectively. Jekeli (2000) and Lee (2009) define the steps for computing σ from the

factory given random walk values of the gyroscopes and accelerometers of the IMUs.

The obtained σ values are shown in the table below for the IMUs HG1700 and HG1900.

Standard Deviations	HG1700	HG1900
$\sigma_a \quad m/s^2$	3.667 x 10-3	3.667 x 10-3
$\sigma_\omega \quad rad/s$	3.636 x 10-5	2.618 x 10-5

Table 3.1. Accelerometer and gyroscope standard deviations of HG1700 and HG1900

The model is nonlinear and after linearization by using the Taylor's series expansion we have,

$$\underset{[n\times m]}{A}\underset{[m\times 1]}{\xi} + \underset{[n\times 3n]}{B}\underset{[m\times 1]}{e} + \underset{[n\times 1]}{w} = \underset{[n\times 1]}{0} \tag{3.27}$$

where ξ is the vector of incremental parameters, and the misclosure vector is

$$w = f\left(Y_{obs}, \Xi_0\right) \tag{3.28}$$

The design matrices are,

$$A = \left.\frac{\partial f(Y, \Xi)}{\partial \Xi}\right|_{\Xi_0, Y_0}$$
$$B = \left.\frac{\partial f(Y, \Xi)}{\partial Y}\right|_{\Xi_0, Y_0} \tag{3.29}$$

where the initial Taylor's series expansion is evaluated about Ξ_0 and Y_0, which symbolize the initial approximate unknown vector and initial observation vector, respectively. The correction vector is

$$\xi = \Xi - \Xi_0 \qquad (3.30)$$

and

$$\hat{\Xi} = \Xi_0 + \hat{\xi} \qquad (3.31)$$

where

$$\hat{\xi} = -N^{-1} A^T C^{-1} w \qquad (3.32)$$

$$C = BP^{-1} B^T \qquad (3.33)$$

and the normal matrix is

$$N = A^T C^{-1} A^T \qquad (3.34)$$

We can estimate the cofactor matrix of the unknowns $Q_{\hat{\xi}}$ by

40

$$Q_{\hat{\xi}} = N^{-1} \tag{3.35}$$

and, the dispersion matrix of the unknowns by

$$D\{\hat{\xi}\} = \hat{\sigma}_0^2 \, Q_{\hat{\xi}} \tag{3.36}$$

where the estimated variance component is

$$\hat{\sigma}_0^2 = \frac{\hat{e}^T P \hat{e}}{n - m} \tag{3.37}$$

where the vector of the estimated random errors is

$$\hat{e} = -P^{-1}B^T C^{-1}\left(w + A\hat{\xi}\right) \tag{3.38}$$

Here, one should notice that in Shin (2002) and Syed et al. (2007), the normal matrix N (equation 3.34) was obtained as

$$N = A^T \left(BP^{-1}B^T\right)^{-1} A^T + P_{\xi}$$

where P_{ξ} is the a priori weight matrix of the unknowns.

41

Including P_ξ can be considered as a stochastic constraint to the system and the

calibration model. The constraint is usually used in order to stabilize the system if there is

any singularity problem in the adjustment calculations (when the system is unstable).

Then the method will be the Gauss-Helmert model with stochastic constraints. However,

in this calibration study, there is no need to use any constraint.

In Shin and El-Sheimy (2002) and in Shin (2001), there are mistakes in the derivation of

the components of the design matrix A for the non-orthogonality errors which cause

singularity problems in the adjustment computations. It was probably the reason for the

authors to use the constraint in the adjustment model. These mistakes will be addressed

after the linearized elements of the design matrix are given (page 49). The linearization

and iteration steps in the calibration estimation are described below.

3.4.1 Linearization Steps

Expanding the adjustment model $f(Y_{obs} - e, \Xi) = 0$ to the Taylor's series about Ξ_0 and Y_0,

and neglecting the higher order terms, gives

$$\left.\frac{\partial f(Y,\Xi)}{\partial \Xi}\right|_{\Xi_0,Y_0} (\Xi - \Xi_0) + \left.\frac{\partial f(Y,\Xi)}{\partial Y}\right|_{\Xi_0,Y_0} (Y - Y_0) + f(\Xi_0, Y_0) = 0 \qquad (3.39)$$

with the expected observation vector Y , we rewrite the vector of the random errors as

$$e = Y - Y_{obs} \qquad (3.40)$$

and then we can write

$$(Y - Y_0) = (Y_{obs} - Y_0) + e \tag{3.41}$$

Thus we get

$$\left. \frac{\partial f(Y,\Xi)}{\partial \Xi} \right|_{\Xi_0,Y_0} (\Xi - \Xi_0) + \left. \frac{\partial f(Y,\Xi)}{\partial Y} \right|_{\Xi_0,Y_0} (Y - Y_{obs})$$

$$+ \left\{ f(\Xi_0,Y_0) + \left. \frac{\partial f(Y,\Xi)}{\partial Y} \right|_{\Xi_0,Y_0} (Y_{obs} - Y_0) \right\} = 0 \tag{3.42}$$

or

$$A\xi + Be + \{f(\Xi_0,Y_0) + B(Y_{obs} - Y_0)\} = 0 \tag{3.43}$$

with

$$w = f(\Xi_0,Y_0) + B(Y_{obs} - Y_0) \tag{3.44}$$

Due to the least squares adjustment solutions $e^T Pe$ is to be minimized and the adjustment solution yields the equation 3.32.

43

3.4.2 Iteration Steps

In the first solution (zeroth iteration) we use $Y_0 = Y_{obs}$ and (3.39) becomes

$$\left. \frac{\partial f(Y,\Xi)}{\partial \Xi} \right|_{\Xi_0, Y_{obs}} (\Xi - \Xi_0) + \left. \frac{\partial f(Y,\Xi)}{\partial Y} \right|_{\Xi_0, Y_{obs}} (Y - Y_{obs})$$
$$+ f(\Xi_0, Y_{obs}) = 0 \tag{3.45}$$

or

$$A\xi_0 + Be_0 + w_0 = 0 \tag{3.46}$$

Here, because $Y_{obs} - Y_0 = 0$, the misclosure vector does not contain the second term and it is obtained as

$$w_0 = f(\Xi_0, Y_{obs}) \tag{3.47}$$

and the adjusted values from the zeroth iteration are estimated by

$$\hat{\Xi}_0 = \Xi_0 + \xi_0 \tag{3.48}$$

$$\hat{Y}_0 = Y_{obs} + e_0 \tag{3.49}$$

44

In the first iteration $\left(\Xi_1, Y_1\right) = \left(\hat{\Xi}_0, \hat{Y}_0\right)$ is taken. Then, we have

$$
\begin{aligned}
&\left.\frac{\partial f(Y, \Xi)}{\partial \Xi}\right|_{\Xi_1, Y_1}\left(\hat{\Xi}_1 - \Xi_1\right) + \left.\frac{\partial f(Y, \Xi)}{\partial Y}\right|_{\Xi_1, Y_1}\left(\hat{Y}_1 - Y_{obs}\right) \\
&+ \left\{ f\left(\Xi_1, Y_1\right) + \left.\frac{\partial f(Y, \Xi)}{\partial Y}\right|_{\Xi_1, Y_1}\left(Y_{obs} - Y_1\right) \right\} = 0
\end{aligned}
\tag{3.50}
$$

or

$$
A\hat{\xi}_1 + B\hat{e}_1 + w_1 = 0
\tag{3.50}
$$

and the least squares solution gives

$$
\hat{\Xi}_1 = \Xi_1 + \hat{\xi}_1
\tag{3.52}
$$

$$
\hat{Y}_1 = Y_{obs} + \hat{e}_1
\tag{3.53}
$$

At the ith iteration, which is the $(i+1)^{\text{th}}$ solution, $\left(\Xi_i, Y_i\right) = \left(\hat{\Xi}_{i-1}, \hat{Y}_{i-1}\right)$ is taken and the equation 3.39 becomes,

$$\frac{\partial f(Y,\Xi)}{\partial \Xi}\bigg|_{\Xi_i,Y_i} \left(\hat{\Xi}_i - \Xi_i\right) + \frac{\partial f(Y,\Xi)}{\partial Y}\bigg|_{\Xi_i,Y_i} \left(\hat{Y}_i - Y_{obs}\right)$$
$$+ \left\{ f(\Xi_i, Y_i) + \frac{\partial f(Y,\Xi)}{\partial Y}\bigg|_{\Xi_i,Y_i} \left(Y_{obs} - Y_i\right) \right\} = 0 \tag{3.54}$$

or

$$A\hat{\xi}_i + B\hat{e}_i + w_i = 0 \tag{3.55}$$

and again the least squares solution gives

$$\hat{\Xi}_i = \Xi_i + \hat{\xi}_i \tag{3.56}$$

$$\hat{Y}_i = Y_{obs} + \hat{e}_i \tag{3.57}$$

During the iteration process, $\hat{\xi}$ should go to zero and $\hat{e}$ should become stable, which means that the solution is converging. After the linearization of the calibration, the coefficient matrices are obtained as follows.

3.4.3 Derivation of the Coefficient Matrices

The design matrices for the 9-parameter solution which considers all 9 errors are

$$A = \begin{bmatrix} \cdots & \cdots & \cdots & \cdots & \cdots & \cdots & \cdots & \cdots & \cdots \\ \dfrac{\partial f}{\partial b_{ax}} & \dfrac{\partial f}{\partial b_{ay}} & \dfrac{\partial f}{\partial b_{az}} & \dfrac{\partial f}{\partial s_{ax}} & \dfrac{\partial f}{\partial s_{ay}} & \dfrac{\partial f}{\partial s_{az}} & \dfrac{\partial f}{\partial \theta_{ayz}} & \dfrac{\partial f}{\partial \theta_{azx}} & \dfrac{\partial f}{\partial \theta_{azy}} \\ \cdots & \cdots & \cdots & \cdots & \cdots & \cdots & \cdots & \cdots & \cdots \end{bmatrix}_{n \times 9} \tag{3.58}$$

$$B = \begin{bmatrix} \cdots & \cdots & \cdots & & & & \\ & & & \dfrac{\partial f}{\partial Y_{ax}} & \dfrac{\partial f}{\partial Y_{ay}} & \dfrac{\partial f}{\partial Y_{az}} & \\ & & & & & & \cdots \quad \cdots \quad \cdots \end{bmatrix}_{n \times 3n} \tag{3.59}$$

The correction vector, the residual vector and the misclosure vectors are

$$\xi = \begin{bmatrix} \xi b_{ax} & \xi b_{ay} & \xi b_{az} & \xi s_{ax} & \xi s_{ay} & \xi s_{az} & \xi \theta_{ayz} & \xi \theta_{azx} & \xi \theta_{azy} \end{bmatrix}^T_{9 \times 1} \tag{3.60}$$

$$e = \begin{bmatrix} \cdots & \cdots & \cdots & e_{ax} & e_{ay} & e_{az} & \cdots & \cdots & \cdots \end{bmatrix}^T_{3n \times 1} \tag{3.61}$$

$$w = \begin{bmatrix} \cdots & f_a(\Xi, Y) & \cdots \end{bmatrix}^T_{n \times 1} \tag{3.62}$$

and linearized elements of the design matrices are

$$\frac{\partial f_a}{\partial b_{ax}} = -\frac{2}{(1+s_{ax})} \begin{bmatrix} a_x + a_y \tan\theta_{ayz} \\ + a_z \left(\tan\theta_{azx} \tan\theta_{ayz} - \tan\theta_{azy} / \cos\theta_{azx} \right) \end{bmatrix} \tag{3.63}$$

$$\frac{\partial f_a}{\partial b_{ay}} = -\frac{2}{(1+s_{ay})} \left(\frac{a_y + a_z \tan\theta_{azx}}{\cos\theta_{ayz}} \right) \tag{3.64}$$

$$\frac{\partial f_a}{\partial b_{az}} = -\frac{2}{(1+s_{az})} \left(\frac{a_z}{\cos\theta_{azx} \cos\theta_{azy}} \right) \tag{3.65}$$

47

$$\frac{\partial f_a}{\partial s_{ax}} = -\frac{2(Y_{ax} - b_{ax})}{(1+s_{ax})^2}\left[\begin{array}{l} a_x + a_y \tan\theta_{ayz} \\ + a_z\left(\tan\theta_{azx}\tan\theta_{ayz} - \tan\theta_{azy}/\cos\theta_{azx}\right)\end{array}\right] \quad (3.66)$$

$$\frac{\partial f_a}{\partial s_{ay}} = -\frac{2(Y_{ay} - b_{ay})}{(1+s_{ay})^2}\left(\frac{a_y + a_z \tan\theta_{azx}}{\cos\theta_{ayz}}\right) \quad (3.67)$$

$$\frac{\partial f_a}{\partial s_{az}} = -\frac{2(Y_{az} - b_{az})}{(1+s_{az})^2}\left(\frac{g_z}{\cos\theta_{azx}\cos\theta_{azy}}\right) \quad (3.68)$$

$$\frac{\partial f_a}{\partial \theta_{ayz}} = 2\left(a_y + a_z \tan\theta_{azx}\right)\left[\frac{a_x}{\cos^2\theta_{ayz}} + \frac{(Y_{ay} - b_{ay})\tan\theta_{ayz}}{(1+s_{ay})\cos\theta_{ayz}}\right] \quad (3.69)$$

$$\frac{\partial f_a}{\partial \theta_{azx}} = 2a_z\left[\begin{array}{l} \left(\dfrac{\tan\theta_{ayz}}{\cos^2\theta_{azx}} - \dfrac{\tan\theta_{azx}\tan\theta_{azy}}{\cos\theta_{azx}}\right)a_x \\[2ex] + \dfrac{(Y_{ay} - b_{ay})}{(1+s_{ay})\cos^2\theta_{azx}\cos\theta_{ayz}} \\[2ex] + \dfrac{(Y_{az} - b_{az})\tan\theta_{azx}}{(1+s_{az})\cos\theta_{azy}\cos\theta_{azx}}\end{array}\right] \quad (3.70)$$

$$\frac{\partial f_a}{\partial \theta_{azy}} = 2a_z\left[\frac{-a_x}{\cos^2\theta_{azy}\cos\theta_{azx}} + \frac{(Y_{az} - b_{az})\tan\theta_{azy}}{(1+s_{az})\cos\theta_{azx}\cos\theta_{azy}}\right] \quad (3.71)$$

$$\frac{\partial f_a}{\partial Y_{ax}} = \frac{2}{(1+s_{ax})}\left[\begin{array}{l} a_x + a_y \tan\theta_{ayz} \\ + a_z\left(\tan\theta_{azx}\tan\theta_{ayz} - \tan\theta_{azy}/\cos\theta_{azx}\right)\end{array}\right] \quad (3.72)$$

$$\frac{\partial f_a}{\partial Y_{ay}} = \frac{2}{(1+s_{ay})}\left(\frac{a_y + a_z \tan\theta_{azx}}{\cos\theta_{ayz}}\right) \quad (3.73)$$

$$\frac{\partial f_a}{\partial Y_{az}} = \frac{2}{(1+s_{az})}\left(\frac{a_z}{\cos\theta_{azx}\cos\theta_{azy}}\right) \quad (3.74)$$

Here, the term $\cos\theta_{ayz}$ in the denominator of the last term in equation 3.69, the term

$\cos\theta_{azx}$ in the denominators of the second and last terms in equation 3.70 and the term

$\cos\theta_{azy}$ in the denominator of the last term in equation 3.71 were missed by Shin and El-

Sheimy (2002).

The design matrices for the bias and scale factor solution (6 unknowns) are

$$
A = \begin{bmatrix}
\cdots & \cdots & \cdots & \cdots & \cdots & \cdots \\
\dfrac{\partial f}{\partial b_{ax}} & \dfrac{\partial f}{\partial b_{ay}} & \dfrac{\partial f}{\partial b_{az}} & \dfrac{\partial f}{\partial s_{ax}} & \dfrac{\partial f}{\partial s_{ay}} & \dfrac{\partial f}{\partial s_{az}} \\
\cdots & \cdots & \cdots & \cdots & \cdots & \cdots
\end{bmatrix}_{n\times 6}
\tag{3.75}
$$

$$
B = \begin{bmatrix}
\cdots & \cdots & \cdots & & & & & & \\
 & & & \dfrac{\partial f}{\partial Y_{ax}} & \dfrac{\partial f}{\partial Y_{ay}} & \dfrac{\partial f}{\partial Y_{az}} & & & \\
 & & & & & & \cdots & \cdots & \cdots
\end{bmatrix}_{n\times 3n}
\tag{3.76}
$$

The correction vector, the residual vector and the misclosure vectors are

$$
\xi = \begin{bmatrix} \xi b_{ax} & \xi b_{ay} & \xi b_{az} & \xi s_{ax} & \xi s_{ay} & \xi s_{az} \end{bmatrix}^T_{6\times 1}
\tag{3.77}
$$

$$
e = \begin{bmatrix} \cdots & \cdots & \cdots & e_{ax} & e_{ay} & e_{az} & \cdots & \cdots & \cdots \end{bmatrix}^T_{3n\times 1}
\tag{3.78}
$$

$$
w = \begin{bmatrix} \cdots & f_a(\Xi, Y) & \cdots \end{bmatrix}^T_{n\times 1}
\tag{3.79}
$$

and linearized elements of the design matrices are

$$\frac{\partial f_a}{\partial b_{ax}} = -\frac{2(Y_{ax} - b_{ax})}{(1 + s_{ax})^2}, \frac{\partial f_a}{\partial b_{ay}} = -\frac{2(Y_{ay} - b_{ay})}{(1 + s_{ay})^2}, \frac{\partial f_a}{\partial b_{az}} = -\frac{2(Y_{az} - b_{az})}{(1 + s_{az})^2} \qquad (3.80)$$

$$\frac{\partial f_a}{\partial s_{ax}} = -\frac{2(Y_{ax} - b_{ax})^2}{(1 + s_{ax})^3}, \frac{\partial f_a}{\partial s_{ay}} = -\frac{2(Y_{ay} - b_{ay})^2}{(1 + s_{ay})^3}, \frac{\partial f_a}{\partial s_{az}} = -\frac{2(Y_{az} - b_{az})^2}{(1 + s_{az})^3} \qquad (3.81)$$

$$\frac{\partial f_a}{\partial Y_{ax}} = \frac{2(Y_{ax} - b_{ax})}{(1 + s_{ax})^2}, \frac{\partial f_a}{\partial Y_{ay}} = \frac{2(Y_{ay} - b_{ay})}{(1 + s_{ay})^2}, \frac{\partial f_a}{\partial Y_{az}} = \frac{2(Y_{az} - b_{az})}{(1 + s_{az})^2} \qquad (3.82)$$

And the design matrices for the bias and scale factor solution are

$$A = \begin{bmatrix} \cdots & \cdots & \cdots \\ \dfrac{\partial f}{\partial b_{ax}} & \dfrac{\partial f}{\partial b_{ay}} & \dfrac{\partial f}{\partial b_{az}} \\ \cdots & \cdots & \cdots \end{bmatrix}_{n \times 3} \qquad (3.83)$$

$$B = \begin{bmatrix} \cdots & \cdots & \cdots & & & & \\ & & & \dfrac{\partial f}{\partial Y_{ax}} & \dfrac{\partial f}{\partial Y_{ay}} & \dfrac{\partial f}{\partial Y_{az}} & \\ & & & & \cdots & \cdots & \cdots \end{bmatrix}_{n \times 3n} \qquad (3.84)$$

the correction vector, the residual vector and the misclosure vectors are

$$\xi = \begin{bmatrix} \xi b_{ax} & \xi b_{ay} & \xi b_{az} \end{bmatrix}_{3 \times 1}^T \qquad (3.85)$$

$$e = \begin{bmatrix} \cdots & \cdots & \cdots & e_{ax} & e_{ay} & e_{az} & \cdots & \cdots & \cdots \end{bmatrix}_{3n \times 1}^T \qquad (3.86)$$

$$w = \begin{bmatrix} \cdots & f_a(\Xi, Y) & \cdots \end{bmatrix}_{n \times 1}^T \qquad (3.87)$$

and linearized elements of the design matrices are

$$\frac{\partial f_a}{\partial b_{ax}} = -2(Y_{ax} - b_{ax}), \quad \frac{\partial f_a}{\partial b_{ay}} = -2(Y_{ay} - b_{ay}), \quad \frac{\partial f_a}{\partial b_{az}} = -2(Y_{az} - b_{az}) \quad (3.88)$$

$$\frac{\partial f_a}{\partial Y_{ax}} = 2(Y_{ax} - b_{ax}), \quad \frac{\partial f_a}{\partial Y_{ay}} = 2(Y_{ay} - b_{ay}), \quad \frac{\partial f_a}{\partial Y_{az}} = 2(Y_{az} - b_{az}) \quad (3.89)$$

By replacing the acceleration components with the rotation rate components in the
equations above, the relevant equations can be obtained for the gyroscope measurements.

3.5 IMU Data Collection Procedure for Calibration

The number of attitudes must be at least as large as the number the error parameters in
order to avoid singularities when the inverse of the normal matrix is being computed.
Even though the gyroscope and accelerometer errors are estimated independently, the
gyroscope data and accelerometer data are collected for the same attitude. Thus, 9 or
more IMU attitude measurements are required in order to be able to estimate the bias,
scale factor and non-orthogonality errors for the gyroscope and accelerometer sensors
located on x, y and z axes. Each attitude should be different to avoid singularities in the
adjustment computations. The possible IMU attitudes are described as each face down (6
attitudes), each side down (12 attitudes) and each corner down (8 attitudes) which gives a
total of 26 different attitudes. The alignments of the IMU axes to specific directions are
not necessary, but they should be significantly different from each other in every attitude.
Some of the attitudes (one sample for each option) are demonstrated in Figure 3.3 which
is a simplified form of Figure 8 of Shin and El-Sheimy (2002).
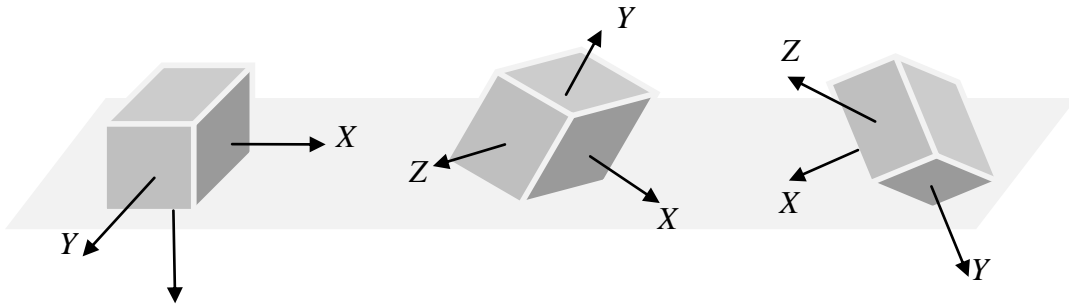
Figure 3.3. Sample IMU attitudes from each face down (left), each side down (center) and each corner down (right)

Chapter 4: Simulation Study

The calibration of a strapdown IMU was performed by using simulation data. For this purpose, the artificial IMU data were generated and the multi-position calibration method was applied to the simulation data.

4.1 Production of the Simulation Data

The IMU basically comprises accelerometer and gyroscope sensors which in the static mode sense components of the Earth rotation and the reactions to gravity vectors, respectively. Thus, the simulation IMU gyroscope data were generated by using the true Earth rotation rate while the mean gravity magnitude data used for producing the accelerometer data. The initial IMU simulation data (first attitude data) were generated for a point at latitude of 40°, corresponding to the Ohio State University campus, in sections 4.1.1 and 4.1.2. Because the calibration method requires numerous IMU attitude measurements, the later attitude data were produced by multiplying the first data with the rotation matrices for desired related angles, (Section 4.2).

4.1.1 Production of the Gyroscope Data

The Earth rotation rate vector is first defined in the Earth frame and then transformed to the navigation frame by multiplying it with the direction cosine matrix (DCM) as shown below.

The Earth rotation rate vector in the Earth frame is

$$\omega_e = \begin{bmatrix} 0 & 0 & \omega_{true} \end{bmatrix}^T \tag{4.1}$$

and it is obtained in the navigation frame as

$$\omega_n = C_e^n \omega_e = \begin{bmatrix} \omega_{true} \cos \omega \\ 0 \\ -\omega_{true} \sin \lambda \end{bmatrix} \tag{4.2}$$

where the true Earth rotation rate is $\omega_{true} = 7.292115 \times 10^{\wedge}\text{-}5$ rad/s and the DCM for

transformation from the Earth frame to navigation frame is

$$C_e^n = \begin{bmatrix} -\sin\varphi\cos\lambda & -\sin\varphi\sin\lambda & \cos\varphi \\ -\sin\lambda & \cos\lambda & 0 \\ -\cos\varphi\cos\lambda & -\cos\varphi\sin\lambda & -\sin\varphi \end{bmatrix} \tag{4.3}$$

where φ is latitude and λ is the longitude. Moreover, computation of the Earth rotation

vector is independent of λ, as it can be seen in 4.2.
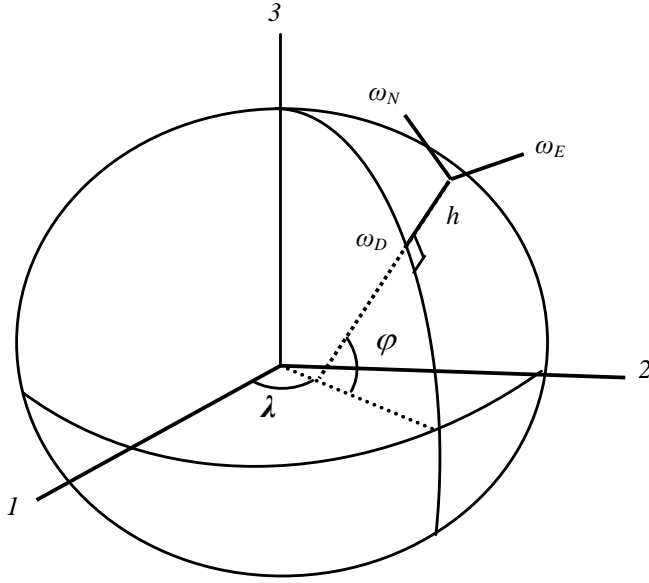
Figure 4.1. Earth rotation rate in the navigation frame (NED)

The navigation frame that was used is a North-East-Down (NED) frame and the body

frame was assumed to be aligned with it. Therefore, the IMU simulation data were not

transformed to any other reference frame. Initially, the x, y and z axes of the IMU were

assumed to be oriented in the North, East and down directions, respectively. Thus, the

Earth rotation rate vector in the navigation frame was used as the gyroscope data for the

first data. The following vector represents the simulated gyroscope data with no errors

and for this first IMU attitude;

$$\underline{\hat{Y}}_\omega = \begin{bmatrix} \omega_x & \omega_y & \omega_z \end{bmatrix}^T_{1\times 3} \tag{4.4}$$

55

where $\hat{\underline{Y}}_\omega$ is the errorless gyroscope observation data vector and ω_i are the sensed

gyroscope values (i = x, y and z).

4.1.2 Production of the Accelerometer Data

In the static mode, the accelerometers in the IMU will sense reactions to the components

of the gravity vector. On a perfectly level surface, the axis corresponding to the down

direction will record the negative gravity magnitude while the horizontal axes will record

zero. By using a mean gravity magnitude for 40° latitude (because the location of the

OSU campus is approximately $\varphi = 40^o$ and $\lambda = -83^o$), the gravity vector for a point in the

navigation frame was generated as,

$$\underline{g}_n = \begin{bmatrix} 0 & 0 & g \end{bmatrix}^T \tag{4.5}$$

where the mean gravity is $g = 9.801 m/s^2$.

The first accelerometer data vector in the NED navigation frame will be

$$\underline{a}_n = \begin{bmatrix} a_x & a_y & a_z \end{bmatrix}^T = -\underline{g}_n \tag{4.6}$$

Then, the errorless accelerometer data vector for the first IMU attitude was produced as

$$\hat{\underline{Y}}_a = \begin{bmatrix} a_x & a_y & a_z \end{bmatrix}^T_{1\times3} \tag{4.7}$$

56

where $\hat{\underline{Y}}_a$ is the errorless observation vector for the accelerometer, a_i are the sensed

accelerometer values corresponding to x, y and z axes of the IMU.

As shown by Shin (2001) in Chapter 4 with experimental estimations, the change in the

reference gravity value only affects the scale factor while it does not have any influence

on the bias. Therefore, the use of a mean gravity magnitude value should be sufficiently

accurate in the accelerometer calibration with both simulated and measured IMU data.

4.2 Generation of the Different IMU Attitude Measurements

After generating the initial data set, the subsequent IMU attitude data were generated by

multiplying the initial data vector by different rotation matrices as shown below.

For example, the errorless data vector for the second IMU attitude measurement, $\hat{\underline{Y}}_{\omega2}$, is

obtained by

$$\hat{\underline{Y}}_{\omega2} = \underline{R}_3(\alpha)\underline{R}_2(\chi)\underline{R}_1(\eta)\underline{Y}_1 = \underline{R}\hat{\underline{Y}}_{\omega1} \tag{4.8}$$

$$\hat{\underline{Y}}_{a2} = \underline{R}_3(\alpha)\underline{R}_2(\chi)\underline{R}_1(\eta)\underline{Y}_1 = \underline{R}\hat{\underline{Y}}_{a1} \tag{4.9}$$

where $\hat{\underline{Y}}_{\omega1}$ and $\hat{\underline{Y}}_{a1}$ are the first IMU attitude data vectors for gyroscope and

accelerometer, and $\underline{R}_1(\eta)$, $\underline{R}_2(\chi)$ and $\underline{R}_3(\alpha)$ are the rotation matrices about the x

(Roll), y (Pitch) and the z (Yaw) axes, respectively. The total transformation matrix $\underline{R}$ is

shown below.

$$\underline{R} = \begin{bmatrix} \cos\alpha\cos\chi & \cos\alpha\sin\chi\sin\eta + \sin\alpha\cos\eta & -\cos\alpha\sin\chi\cos\eta + \sin\alpha\sin\eta \\ -\sin\alpha\cos\chi & -\sin\alpha\sin\beta\sin\eta + \cos\alpha\cos\eta & \sin\alpha\sin\chi\cos\eta + \cos\alpha\sin\eta \\ \sin\chi & -\cos\chi\sin\eta & \cos\chi\cos\eta \end{bmatrix}$$

(4.10)

By using the same methodology, the remaining data sets were generated with different axes orientations. The attitudes were generated in such a way that the IMU axes were pointing to a different direction in every attitude measurement. For example, it was attempted that each gyroscope and accelerometer on an IMU axis would sense $+$ and $-$ the same (or similar) value of the corresponding Earth rotation rate vector and acceleration components, respectively.

Moreover, in order to simulate the real field situation and therefore avoid perfect up and down IMU axes orientations, which is not possible and without a precise instrument, rotation angles were deformed by adding random angular values with standard deviation of 2°. Furthermore, 20° offset from the main geographical directions (N, E, and D) was considered in the attitude orientations.

Twenty-six IMU attitude data sets were generated with the attitudes that each face (6 attitudes), each edge (12 attitudes) and each corner (8 attitudes) of the IMU box was pointing down. Then the HG1700 factory defined errors were included in the errorless data sets as explained in the next section.

Each IMU attitude data set was aimed to be 3 minutes long and has the frequency of 1 Hz (1 data per second). A single attitude data, whose dimension was 3x1, was replicated

58

$l = 180$ times within a vector and thus a three-minute-long IMU attitude data set with the dimension of 3xl was generated for each IMU attitude.

4.3 Inclusion of the Errors in the Errorless IMU Simulation Data

The simulated IMU data were corrupted with the inclusion of errors. The deterministic IMU errors were chosen from the parameters defined by the manufacturer for the Honeywell HG1700 (Figure 2.8). Moreover, Gaussian random noise data with mean equal to zero and the standard deviation values given in Table 3.1 were generated in MATLAB. By using the equations 3.13 and 3.17, the chosen biases, scale factor errors and non-orthogonality errors were included in the simulated data, and then the generated random noise values were added to the data.

The related error parameters are shown in Table 4.1.

	Gyroscope	Accelerometer
Bias	4.848E-06 rad/s ($= 1$ °$/hr$)	0.01 m/s2
Scale Factor	150 ppm	300 ppm
Non-orthogonality	100 µ rad	100 µ rad
White Noise	$\sigma_\omega = 3.636\text{x}10^{-5}\ rad/s$	$\sigma_a = 3.667\ \text{x}\ 10^{-3}\ m/s^2$

Table 4.1. Given error parameters for HG1700

The calibration results are presented in the section below.

4.4 Calibration Results of the Simulated IMU Measurements

All twenty-six simulated gyroscope and accelerometer IMU attitude data sets defined

above were used in order to test the multi-position calibration method. After including the

defined error parameters, the data corresponding to the sensor triad were averaged within

each attitude, which yields a 3x1 vector for each attitude that was then used in the

calibration estimations. After the averaging, the gyroscope and accelerometer white noise

variance for the averages will be estimated by

$$\sigma_{\omega-average} = \sigma_{\omega} / \sqrt{n} \qquad (4.11)$$

$$\sigma_{a-average} = \sigma_{a} / \sqrt{n} \qquad (4.12)$$

where n is the number of observations. Here one should notice that the gyroscope and

accelerometer data are calibrated separately in the multi-position calibration method.

Three different scenarios were tried, including no noise in the data, including a defined

level of noise in the data, and including the noise in the data together with increasing the

reference rotation rate by multiplying by 10^4.

The weight matrix P is obtained by the equation 3.26 with using the standard deviation

values from 4.11 and 4.12. Then, the gyroscope and accelerometer error calibration

results were obtained after 100 iterations of the linear least-squares solution. The

calibration results are presented in Sections 4.4.1 and 4.4.2.

4.4.1 Gyroscope Calibration Results

All 3 scenarios mentioned above were tested for the gyroscope simulation data in this section. Table 4.2 includes calibration results of the bias-only solution while 6-parameter and 9-parameter solution results are presented in Table 4.3 and Table 4.4, respectively. Estimated values and absolute differences calculated by equation 4.12 are shown in the following tables.

$$Difference \ (\Delta) = |estimated \ value - true \ value| \qquad (4.12)$$

The values below show the parameters used in the calibration estimations.

Case 1: $\omega = \omega_e$ & $\sigma = 0$

Case 2: $\omega = \omega_e$ & $\sigma_\omega = 3.636 \times 10^{-5} \, rad/s$

Case 3: $\omega = 10^4 \times \omega_e$ & $\sigma_\omega = 3.636 \times 10^{-5} \, rad/s$

	Gyroscope	Case 1			Case 2			Case 3		
		$\omega_{estimated}$	$\sigma_{\omega-est}$	Δ_ω	$\omega_{estimated}$	$\sigma_{\omega-est}$	Δ_ω	$\omega_{estimated}$	$\sigma_{\omega-est}$	Δ_ω
Bias (rad/s)	$b_{\omega x}$	4.85E-06	4.04E-09	2.77E-09	5.12E-06	1.07E-06	2.69E-07	-2.26E-05	4.07E-05	2.74E-05
	$b_{\omega y}$	4.85E-06	4.24E-09	3.53E-09	5.32E-06	1.11E-06	4.77E-07	4.06E-05	4.27E-05	3.57E-05
	$b_{\omega z}$	4.85E-06	4.78E-09	4.04E-10	5.37E-06	1.27E-06	5.25E-07	9.37E-06	4.82E-05	4.52E-06

Table 4.2. 3-parameter (bias-only) solution results of the gyroscope calibration

	Gyroscope	Case 1			Case 2			Case 3		
		$\omega_{estimated}$	$\sigma_{\omega-est}$	Δ_ω	$\omega_{estimated}$	$\sigma_{\omega-est}$	Δ_ω	$\omega_{estimated}$	$\sigma_{\omega-est}$	Δ_ω
Bias (rad/s)	$b_{\omega x}$	4.85E-06	1.35E-09	2.68E-11	5.44E-06	1.15E-06	5.88E-07	5.22E-06	1.36E-05	3.77E-07
	$b_{\omega y}$	4.85E-06	1.46E-09	6.83E-11	4.87E-06	1.25E-06	1.96E-08	5.44E-06	1.47E-05	5.94E-07
	$b_{\omega z}$	4.85E-06	1.56E-09	4.19E-10	5.08E-06	1.33E-06	2.36E-07	8.04E-07	1.57E-05	4.04E-06
Scale Factor Error (ppm)	$s_{\omega x}$	138.453	24.487	11.547	7584.798	20859.022	7434.798	138.988	24.579	11.012
	$s_{\omega y}$	165.556	26.514	15.556	25467.152	22505.033	25317.152	168.235	26.613	18.235
	$s_{\omega z}$	178.691	26.228	28.691	4701.523	22716.690	4551.523	178.962	26.327	28.962

Table 4.3. 6-parameter (bias and scale factor error) solution results of the gyroscope calibration

	Gyroscope	Case 1			Case 2			Case 3		
		$\omega_{estimated}$	$\sigma_{\omega-est}$	Δ_ω	$\omega_{estimated}$	$\sigma_{\omega-est}$	Δ_ω	$\omega_{estimated}$	$\sigma_{\omega-est}$	Δ_ω
Bias (rad/s)	$b_{\omega x}$	4.85E-06	4.02E-21	0.00E+00	5.59E-06	1.22E-06	7.37E-07	5.86E-06	1.21E-06	1.01E-06
	$b_{\omega y}$	4.85E-06	5.32E-21	0.00E+00	4.56E-06	1.71E-06	2.92E-07	4.52E-06	1.60E-06	3.24E-07
	$b_{\omega z}$	4.85E-06	5.24E-21	1.02E-20	3.90E-06	1.65E-06	9.46E-07	3.86E-06	1.58E-06	9.93E-07
Scale Factor Error (ppm)	$s_{\omega x}$	150.000	6.95E-11	7.80E-11	13557.915	21834.303	13407.915	150.806	2.090	0.806
	$s_{\omega y}$	150.000	7.63E-11	6.99E-12	26758.403	23599.707	26608.403	152.725	2.296	2.725
	$s_{\omega z}$	150.000	8.09E-11	5.90E-11	1580.785	25237.662	1430.785	149.494	2.434	0.506
Non-orth. Error (μrad)	$\theta_{\omega yz}$	100.000	1.33E-10	6.60E-11	-32323.790	36613.218	32423.790	97.081	4.007	2.919
	$\theta_{\omega zx}$	100.000	2.30E-10	7.18E-11	-30309.263	70860.251	30409.263	97.016	6.905	2.984
	$\theta_{\omega zy}$	100.000	1.60E-10	3.79E-12	74513.200	47886.190	74413.200	107.945	4.821	7.945

Table 4.4. 9-parameter solution results of the gyroscope calibration

The estimated parameters $\omega_{estimated}$ symbolize the estimated gyroscope errors while

$\sigma_{\omega-est}$, obtained by using the equation 3.36, represents the accuracy and Δ_ω denotes the

absolute error of the estimations in the table above. When there is no white noise in the

data (Case 1), all 9 parameters can be estimated perfectly with the 9-parameter solution.

However, with the defined level of white noise in the data (Case 2), only the gyro bias

can be estimated with reasonable accuracy, and the 3-parameter solution provides more

precise gyro bias estimations according to the standard deviations. On the other hand, the

actual errors showed mixed results. Nevertheless, it is possible to obtain accurate

estimations of all 9 parameters for the data with the defined level of white noise when the

reference Earth rotation rate is increased by 10^4 (Case 3). This is consistent with results

of Syed et al (2007), who claimed that the true Earth rotation rate is so weak that it

cannot be used for calibrating the gyroscope scale factor errors and non-orthogonality

errors and who solved this problem by using a single axis turn table for the gyroscope

calibration.
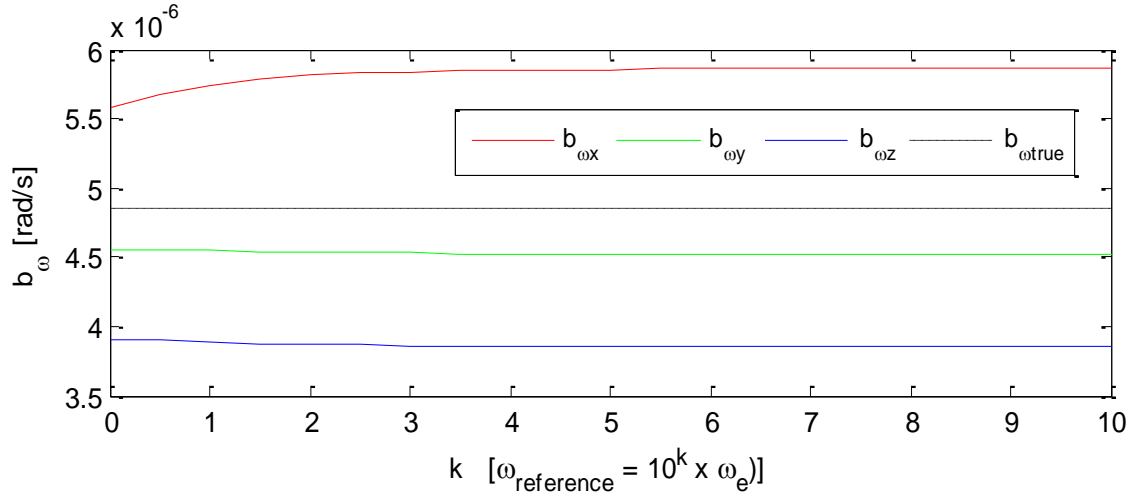
A
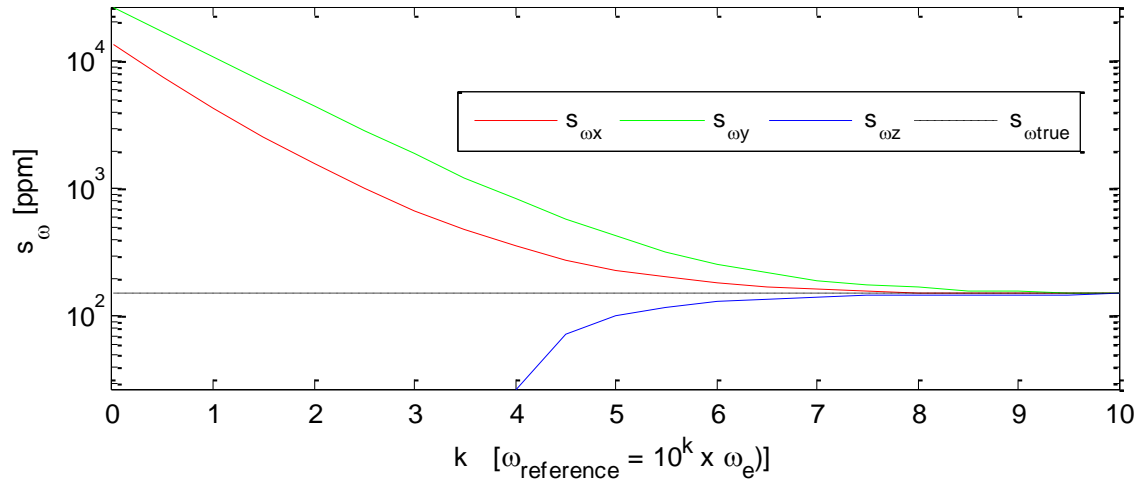
B   continued

Figure 4.2. Estimations of the gyroscope bias (A), scale factor (B), and non-orthogonality (C) errors due to the increase in the reference rotation rate ($\sigma_\omega = 3.636 \times 10^{-5} \ rad/s$)

Figure 4.2 continued
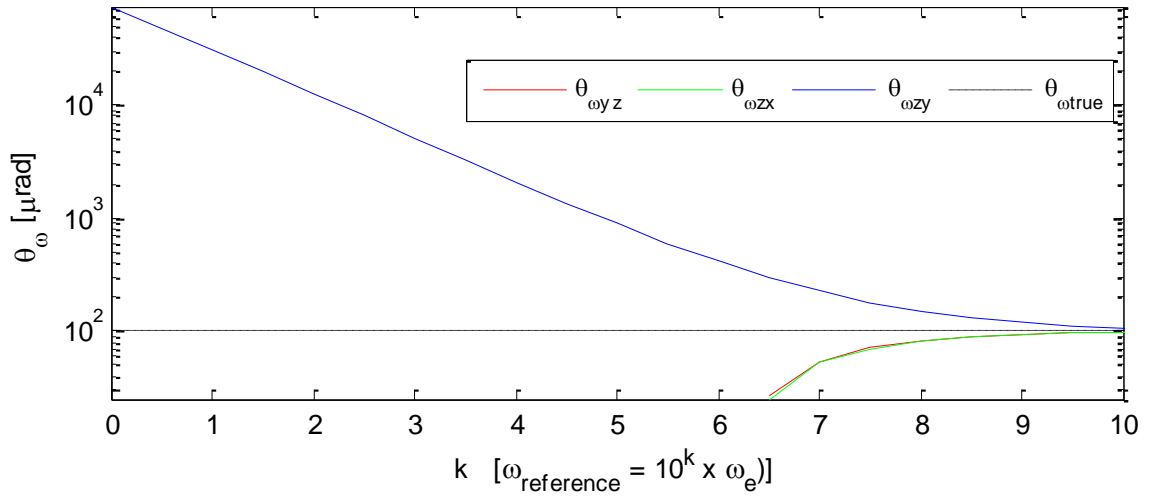
C

As it can be seen from the figures above, estimation accuracies of the gyroscope scale factor and non orthogonality errors increase with the increase in the reference signal. However, the bias estimation accuracy slightly decreases and then becomes constant. We can conclude that the increase in the reference signal has a positive effect on the scale factor error and non-orthogonality estimations while it does not change the bias results very much.

The following figure includes the error estimation results with respect to increase in the white noise level in the IMU simulation data.

A
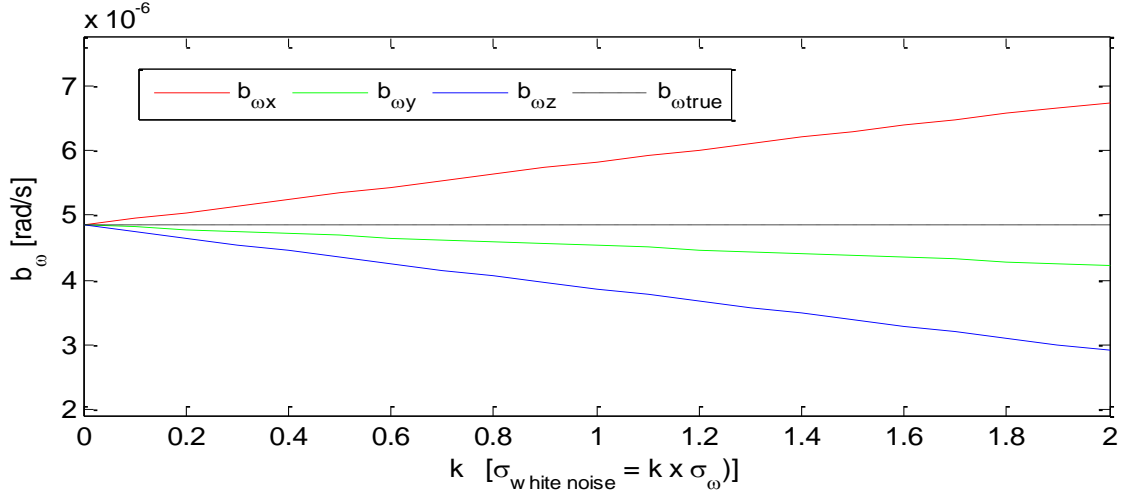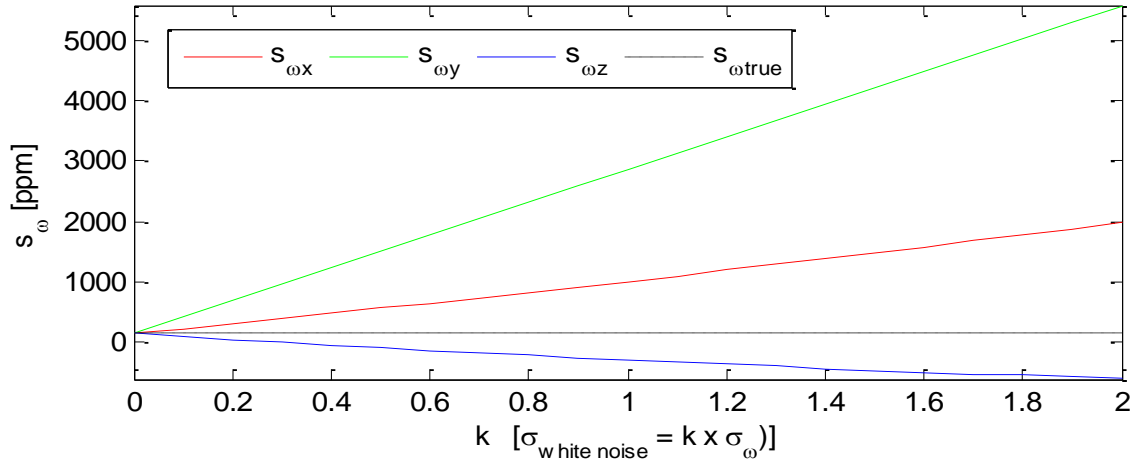
Figure 4.3. Estimations of the gyroscope bias (A), scale factor (B), and non-orthogonality (C) errors due to the increase in the level of gyro white noise ($\sigma_\omega = 3.636 \times 10^{-5}\ rad/s$)

Figure 4.3 continued
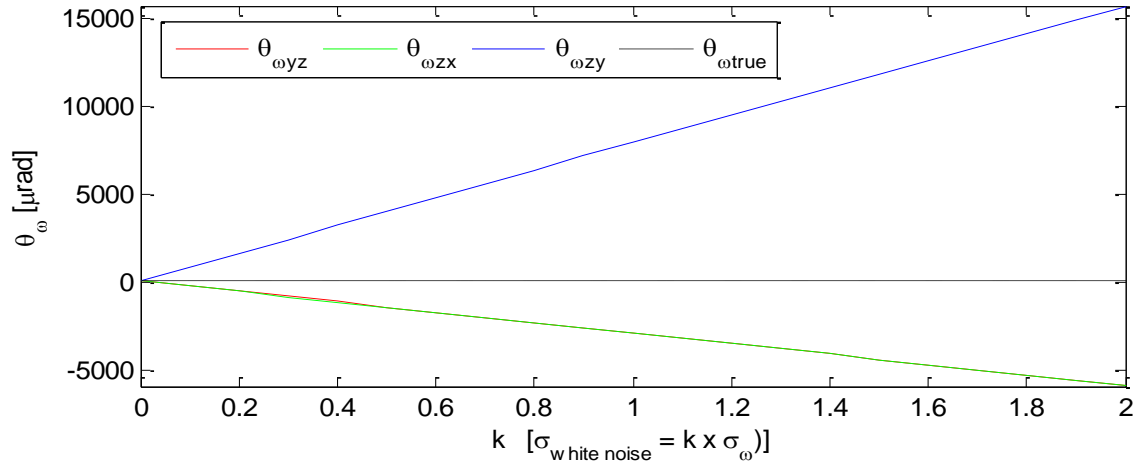
C

It was experienced in this section that the increase in the noise level in the IMU data significantly decreases the error estimation accuracy.

4.4.2 Accelerometer Calibration Results

Only 2 scenarios were tested for the accelerometer data, which uses the simulated data with and without the noise. Because the accelerometer data provided accurate results by using the mean gravity magnitude, there was no need to increase the reference gravity signal. Moreover, only the 9-parameter solution results were presented below since similar results are obtained in the 3- & 6-parameter solutions.

		Case 1: $\sigma_a = 0 \ m/s^2$ $g = g_{mean} = 9.801 \ m/s^2$			Case 2: $\sigma_a = 3.667 \times 10^{-3} \ m/s^2$ $g = g_{mean} = 9.801 m/s^2$		
Accelerometer		$a_{estimated}$	σ_{a-est}	Δ_a	$a_{estimated}$	σ_{a-est}	Δ_a
Bias (m/s^2)	b_{ax}	0.010	4.35E-16	1.51E-16	9.970E-03	1.32E-04	2.97E-05
	b_{ay}	0.010	3.66E-16	1.91E-16	1.005E-02	1.11E-04	4.69E-05
	b_{az}	0.010	3.75E-16	9.91E-16	1.009E-02	1.14E-04	8.97E-05
Scale Factor Error (ppm)	s_{ax}	300.000	6.00E-11	4.60E-11	298.415	18.201	1.585
	s_{ay}	300.000	4.82E-11	4.50E-11	307.166	14.636	7.166
	s_{az}	300.000	5.19E-11	1.99E-12	299.282	15.737	0.718
Non-orth. Error (µrad)	θ_{ayz}	100.000	1.05E-10	2.50E-11	127.802	32.018	27.802
	θ_{azx}	100.000	8.74E-11	6.20E-11	102.237	26.538	2.237
	θ_{azy}	100.000	9.51E-11	1.10E-11	92.445	28.874	7.555

Table 4.5. 9-parameter solution results of the accelerometer calibration

where σ_{a-est} and Δ_a represent the accuracy and absolute error of the accelerometer error

estimations.

The simulation study results showed that the accelerometer errors can accurately be

estimated with current factory defined parameters included in the data. Moreover, the

standard deviation and absolute error estimates were consistent due to the increase in

noise level in the data.

4.5 Summary

Simulation results showed that with a significant number of attitude measurements, all 9

accelerometer errors can be estimated accurately. In all cases, the estimated standard

deviations and absolute errors of the gyro bias estimates are generally consistent (within

an order of magnitude). However, it is only possible to obtain accurate gyroscope scale

factor error and non-orthogonality error estimations if we increase the reference signal strength or decrease the noise in the data (Case 3). Then also, the estimated standard deviations are reasonable. This study has shown that if the gyroscope data have very high level noise (e.g. HG1700 type of IMU), then the Earth rotation rate is not large enough to estimate gyro scale factor and non orthogonality errors. A single axis turntable, which generates rotations at least about 10^4 times greater than the true Earth rotation rate, will help to solve this problem. Moreover, using longer duration attitude data might increase the estimation accuracy as well as using more attitude data, and it should be tested in the real data study. Because the gyro scale factor and non-orthogonality errors cannot be estimated with the Earth rotation rate, the bias-only solution should be used for calibrating gyroscopes of the IMUs, such as HG1700 and HG1900. The effects of the unconsidered errors (scale factor and non-orthogonality errors) in this case might be distributed in the estimated bias results. As it is addressed in Section 3.4, it is believed that the mistakes in the derivations of the design matrix (A) components caused Shin and El-Sheimy (2002) caused them to include the a priori weight matrix of the unknowns (P_ξ) in order to regularize an otherwise singular system. However, having solved the problems in the coefficient matrix components, there is no need to use P_ξ unless we have actual a priori information about the weights of the unknowns.

Chapter 5: Calibration Performance Analyses

To analyze the positioning performance of the multi-position calibration method applied

the two tactical grade IMUs, Honeywell HG1700 and HG1900, a field test was

performed in the west campus parking lot of the Ohio State University on June 06, 2009.

The relevant instruments were installed on a 4-wheel cart, which is then called Cart

Based Geolocation System, for the kinematic measurement. Section 5.1 describes the

equipment included in the calibration test, Section 5.2 presents the test scenarios, and the

estimates of the IMU deterministic errors (bias, scale factor error and non-orthogonality

errors) are given in Section 5.3. Moreover, Section 5.4 shows the accuracy analyses of

the field test while the results are summarized in Section 5.5.

5.1 Cart Based Geolocation System Configuration

The cart based geolocation system is shown in Figure 5.1 and the detailed equipment list

is given in Table 5.1.
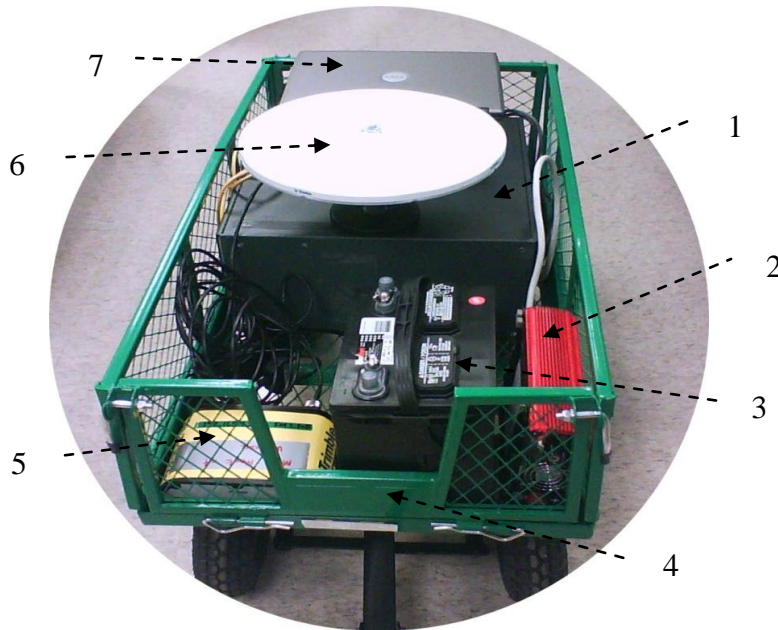
Figure 5.1. Cart Based Geolocation System

1-	IMU Box: a- Honeywell HG1700: a light weight and low cost ring-laser based strap-down Inertial Measurement Unit (IMU) designed for navigation purposes especially for missile guidance and unmanned vehicles (UAV). HG1700 includes three miniature GG1308 Ring Laser Gyroscopes (RLGs) and three RBA-500 Resonating Beam Accelerometers, and low-cost Intel 87C196KC micro-processor b- Honeywell HG1900: a MEMS (Micro electrical Mechanical System) based IMU used for the same purposes as HG1700 and is somewhat less accurate. HG1900 uses MEMS gyros and RBA500 accelerometers, and it requires very low power
2-	AC/DC converter
3-	12V Car Battery
4-	INS Cart: a 4-wheel cart can be pulled by hand or any vehicle
5-	Trimble NETRS GPS receiver
6-	Trimble Zephyr Geodetic II GPS antenna
7-	Laptop Computer, including a PCMCI card connecting the IMUs and the decoding software

Table 5.1. The detailed equipment list of the Cart Based Geolocation System

The original Honeywell hardware system of the IMUs requires an ISA card which cannot

be installed on the modern desktop computers, and, of course, the laptop computers.

Moreover, the software provided by Honeywell can only be executed on Ms DOS

operating system and it is only possible to record 100,000 rows of data, which is equal to

16.7m of data with 100Hz. In order to overcome the limitations of the hardware and

software systems, a PCMCI card is included in the system and a C++ based data

recording software was developed by Jong Ki Lee, researcher in The Geodetic Science

division of OSU, which can operate on Windows XP and can record unlimited amount of

IMU data. These new software and hardware systems enable the use of a laptop computer

for the cart-based geolocation system, which decreases the volume and weight of the

system as well as the power consumption.

The block diagrams of the original Honeywell and the new hardware systems are given

below (Lee, 2009).
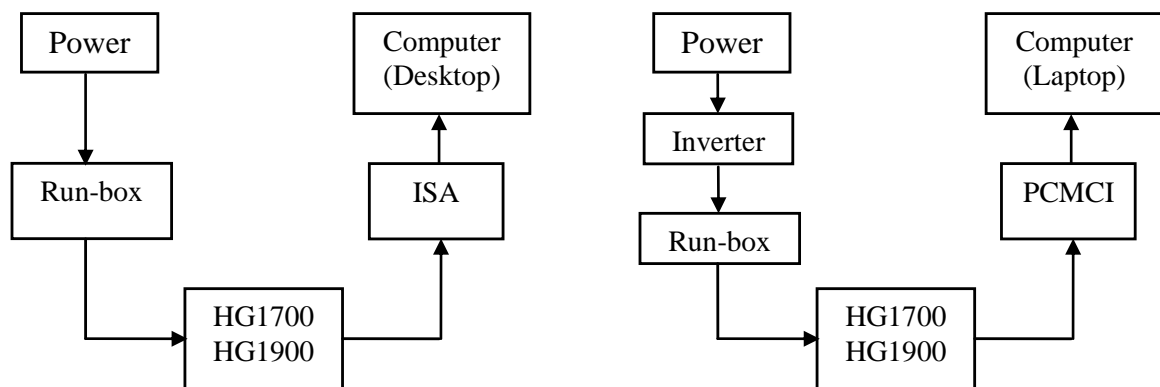
Figure 5.2. The block diagram of the Honeywell hardware system (left) and the
new hardware system (right)

5.2 Performance Test Scenario

Initially 20 minutes of warming up time preceded the measurements. 26 different 5-minute long static IMU attitude measurements were collected for estimation of the IMU bias, scale factor error and non-orthogonality errors. The IMU attitudes included each face down (6 attitudes), each edge down (12 attitudes) and each, corner down (8 attitudes). Then, the IMU box was installed on the cart together with the GPS receiver and the remaining instruments, producing the cart based geolocation system. The GPS measurement and positioning intervals were set equal to 0.1 second. Moreover, another GPS receiver, the base station, was installed at a local control point and its measurement interval was set to 0.1 second. After that, the INS cart was pulled by hand about 25 minutes with a walking speed, and a sweep like trajectory (see Figure 5.2) was followed among the parking space lines. The trajectory included 25 straight sections and 25 very short and sharp curved sections.
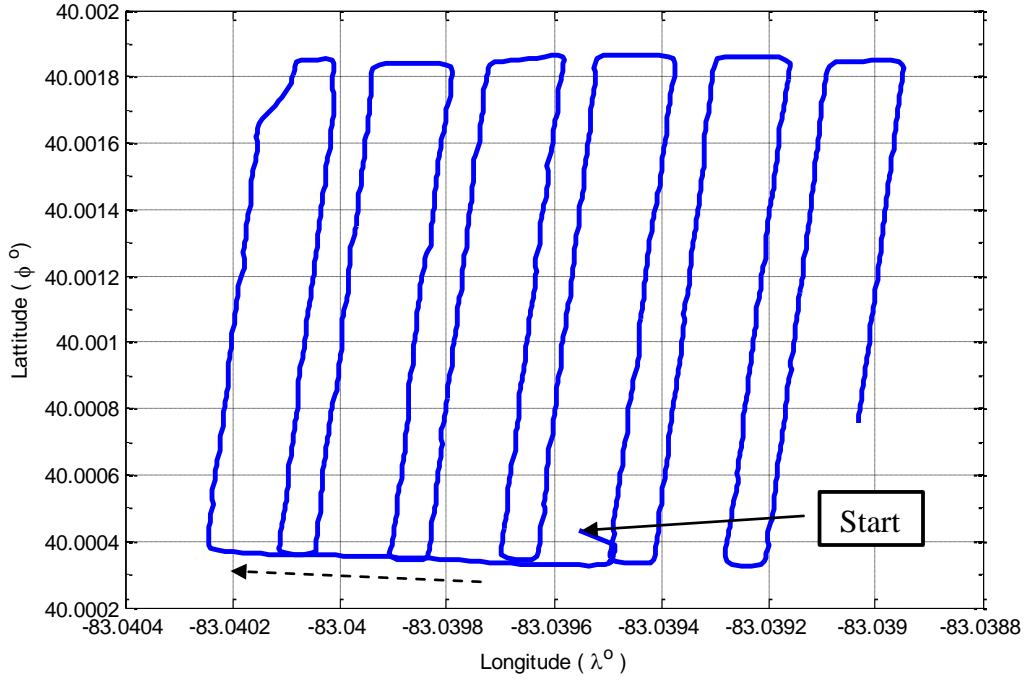
Figure 5.3. GPS trajectory map of the field IMU calibration test

5.3 Calibration Estimates

The HG1900 and HG1700 deterministic errors were calculated as explained in Section 3, and the gyroscope and accelerometer error estimates are presented in this section. Since measurements for 9 IMU attitudes are enough to estimate 9 unknowns (3 biases, 3 scale factor errors and 3 non-orthogonality errors, which are for inertial sensors on the x, y and z axes), and 26 IMU attitudes were done in the field prior the kinematic survey, 4 scenarios were considered to analyze the estimation. In Scenario 1, all 26 IMU attitudes are used, while the first 18 and the first 10 attitudes were used in Scenario 2 and Scenario 3, respectively. Finally, because there were 16 attitude measurements (they took about 80

minutes) remaining after the first 10 attitudes, the last 10 attitude data were included in

Scenario 4 in order to see if the calibration estimates are reliable for IMU measurements

after a long break. Moreover, in order to analyze the required time length (t) for the IMU

attitude measurements, the IMU deterministic errors are estimated for $t=1$minute,

$t=3$minutes and $t=5$minutes for each IMU attitude. Section 5.3.1 includes the error

estimates for gyroscope, and the accelerometer error estimates are presented in Section

5.3.2 for the HG1700 and HG1900.

5.3.1 Gyroscope Error Estimates

As it was claimed by Shin (2002) and Syed et al (2007) and also experienced in Section 4

with a simulation study, gyroscope scale factor errors and non-orthogonality errors were

expected to be very large (unestimable) unless the reference rotation rate is increased.

However, in order to analyze the effects of using or not using the very large estimated

scale factor errors and non-orthogonality errors, the gyroscope errors of the HG1700 and

HG1900 are calculated by using the 3-parameter (bias-only) and 9-parameter (including

all 9 errors) solutions.

Parallel to the results in the simulation study (Chapter 4.4.1), the 3-parameter solution

provided more accurate gyroscope bias estimations than the 9-parameter solution based

on the standard deviations. However, the 9-parameter solution estimated more accurate

gyro biases for the HG1700 when Scenarios 2, 3 and 4 with $t=1$ minute were used, and

for HG1900 results when Scenario 3 was used. Within the 3-parameter solution results,

Scenario 3 and $t=5$ minutes for the HG1700, and Scenario 1 and $t=1$ minute for the

HG1900 provided the most accurate gyroscope bias estimations. When the 9-parameter

solution was used, Scenario 3 yielded the most accurate gyroscope bias estimations when

$t=5$ minutes for HG1700 and $t=3$ minutes for HG1900 for the 9 gyroscope errors.

Moreover, HG1700 bias estimates had smaller standard deviations than the HG1900

results for both 3-parameter and 9-parameter solutions.

As a result, it can be said that Scenario 3 provided the best gyroscope bias estimates

among the scenarios according to the standard deviations even though there is not a

consistent relationship (e.g. accuracy increase or decrease due to the increase in used

attitude numbers or attitude data recording times) among the scenarios.

Gyroscope bias estimates of Scenario 3 for the 3-parameter and 9-parameter solutions are

presented on the tables below. The results of the remaining 3 scenarios are presented in

Appendix A.

Scenario 3: 10 attitudes			t = 1m		t = 3m		t = 5m	
			Estimates	σ	Estimates	σ	Estimates	σ
Bias (rad/s)	HG1700	$b_{\omega x}$	2.46E-06	8.79E-07	2.20E-06	8.55E-07	2.43E-06	6.73E-07
		$b_{\omega y}$	-1.64E-07	8.56E-07	-1.82E-06	8.28E-07	-2.35E-06	6.53E-07
		$b_{\omega z}$	-8.81E-07	8.55E-07	-1.64E-06	7.99E-07	-8.47E-07	6.26E-07
	HG1900	$b_{\omega x}$	-5.97E-06	2.38E-06	-7.08E-06	2.67E-06	-7.39E-06	2.93E-06
		$b_{\omega y}$	1.42E-05	2.30E-06	1.33E-05	2.67E-06	1.21E-05	2.98E-06
		$b_{\omega z}$	9.22E-06	2.10E-06	7.93E-06	2.37E-06	7.58E-06	2.63E-06

Table 5.2. 3-parameter solution gyroscopes error estimates of the HG1700 and HG1900
for Scenario 3

Scenario 3: 10 attitudes			t = 1m		t = 3m		t = 5m	
			Estimates	σ	Estimates	σ	Estimates	σ
HG1700	Bias (rad/s)	$b_{\omega x}$	1.36E-07	6.62E-07	2.77E-06	2.66E-06	3.24E-06	5.30E-07
		$b_{\omega y}$	1.36E-06	5.92E-07	-2.00E-06	2.58E-06	-2.55E-06	5.49E-07
		$b_{\omega z}$	-2.51E-06	5.98E-07	-1.23E-06	1.95E-06	-7.29E-07	4.06E-07
	Scale Fac. (ppm)	$s_{\omega x}$	12696.07	11553.97	7194.42	57380.27	-6802.27	11414.08
		$s_{\omega y}$	18284.77	10245.42	35019.72	58329.83	46239.64	12536.48
		$s_{\omega z}$	29051.21	13881.55	-32018.05	54786.06	-26618.01	11095.15
	Non-orth. (μrad)	$\theta_{\omega yz}$	88220.60	15475.40	-33982.95	74133.32	-43530.31	15316.33
		$\theta_{\omega zx}$	16548.94	13482.97	-17138.50	62597.35	-15627.59	13048.52
		$\theta_{\omega zy}$	53794.20	15419.74	-30793.73	58939.16	-15564.28	12073.05
HG1900	Bias (rad/s)	$b_{\omega x}$	-6.08E-06	1.27E-06	-7.06E-06	7.49E-07	-6.58E-06	1.33E-06
		$b_{\omega y}$	1.36E-05	2.24E-06	1.26E-05	1.54E-06	9.21E-06	3.43E-06
		$b_{\omega z}$	6.43E-06	1.20E-06	4.23E-06	7.85E-07	3.63E-06	1.58E-06
	Scale Fac. (ppm)	$s_{\omega x}$	-76769.15	26086.60	-94917.32	15041.21	-116474.58	27473.59
		$s_{\omega y}$	178213.85	42989.82	191292.65	27625.32	225146.73	60942.90
		$s_{\omega z}$	3511.57	28535.36	49431.94	19360.79	50519.87	38204.54
	Non-orth. (μrad)	$\theta_{\omega yz}$	70402.10	40113.45	75893.20	25119.70	30569.96	49964.45
		$\theta_{\omega zx}$	-2464.51	46613.04	-7034.14	30193.64	-32440.85	63659.29
		$\theta_{\omega zy}$	77572.88	37921.54	81540.91	22666.41	56813.74	41710.64

Table 5.3. 9-parameter solution gyroscope error estimates of the HG1700 and HG1900 for Scenario 3

5.3.2 Accelerometer Error Estimates

Because the accelerometer errors can be estimated by the Multi-Position Calibration Method, the accelerometer deterministic errors are calculated by using only the 9-parameter solution. Scenario 3 and t=3minutes again provided the smallest standard deviations and therefore the most precise estimations. Moreover, the HG1700 results

were slightly more accurate than the HG1900 results in calculating most of the error

parameters. The 9-parameter accelerometer error estimates of Scenario 3 are given in the

table below. The remaining results are presented in Appendix B.

9-Parameter Solution			t = 1m		t = 3m		t = 5m	
			Estimates	σ	Estimates	σ	Estimates	σ
HG1700	Bias (m/s²)	b_{gx}	4.62E-03	1.87E-04	4.92E-03	5.08E-05	4.86E-03	2.38E-04
		b_{gy}	1.94E-03	2.18E-04	-1.17E-04	5.97E-05	-4.34E-04	2.81E-04
		b_{gz}	5.13E-03	1.96E-04	4.23E-03	5.35E-05	3.82E-03	2.51E-04
	Scale Fac. (ppm)	s_{gx}	-107.34	19.38	-130.33	5.26	-120.80	24.64
		s_{gy}	824.25	50.50	344.45	9.93	291.50	45.21
		s_{gz}	418.88	38.67	145.73	7.09	110.90	32.03
	Non-orth. (μrad)	θ_{gyz}	1108.02	53.12	279.48	14.63	196.95	68.74
		θ_{gzx}	18873.33	1275.41	6637.68	346.20	5542.92	1628.29
		θ_{gzy}	-1127.91	94.80	-443.23	26.06	-296.92	122.52
HG1900	Bias (m/s²)	b_{gx}	-4.80E-03	7.73E-05	-4.67E-03	5.41E-05	-4.50E-03	1.72E-04
		b_{gy}	-4.20E-03	9.41E-05	-4.11E-03	6.61E-05	-3.84E-03	2.11E-04
		b_{gz}	1.77E-03	8.34E-05	1.81E-03	5.85E-05	1.81E-03	1.86E-04
	Scale Fac. (ppm)	s_{gx}	-51.64	8.04	-60.37	5.63	-71.34	17.92
		s_{gy}	39.87	20.98	58.36	15.06	112.58	51.06
		s_{gz}	182.05	10.15	175.54	6.92	158.18	20.36
	Non-orth. (μrad)	θ_{gyz}	-39.78	24.26	-36.60	16.96	15.26	53.67
		θ_{gzx}	-2713.96	626.10	-1960.96	440.56	187.88	1411.44
		θ_{gzy}	305.94	45.13	254.70	31.71	106.06	101.20

Table 5.4. 9-parameter solution accelerometer error estimates of the HG1700 and
HG1900 for Scenario 3

5.4 Positioning Accuracy Analyses

Effects of the estimated IMU error parameters on positioning accuracy were analyzed in this section. Each scenario result was used in estimating the positioning accuracy when there were 2s GPS signal outages. The estimated gyroscope and accelerometer errors for the defined scenarios were used as initial estimates in a 27 state Extended Kalman Filter (EKF), developed by Lee (2009). Moreover, standard deviations of the initial IMU states were taken from the least-squares solution (equation 3.36). Positioning errors and their accuracies were determined by comparing the estimated trajectory during GPS outages and the true GPS trajectory. Since the INS and GPS times were synchronized, every unused (not employed for the EKF) GPS position which was obtained during the GPS signal outage time (Figure 5.4) was compared with the corresponding INS position. In addition, because the curved sections are very short, very sharp and the motion is very slow (walking speed), the accuracy estimations were not separated as curved and straight sections and the navigation data was processed as a whole.

The position error vector is obtained by

$$Z = (Z_x, Z_y, Z_h) \qquad (5.1)$$

where x, y are the horizontal coordinates and h is the height, and

$$Z_x = (x_{INS} - x_{GPS}),\ Z_y = (y_{INS} - y_{GPS}),\ Z_h = (h_{INS} - h_{GPS}) \qquad (5.2)$$

The standard deviation of the positioning error (σ_Z) is computed by

$$\sigma_Z = \sqrt{\sigma_{Z,x}^2 + \sigma_{Z,y}^2 + \sigma_{Z,h}^2} \qquad (5.3)$$

where

$$\sigma_{Z,x} = \sqrt{\sum_{i=1}^{n}\left(Z_x^i - \overline{Z}_x\right)^2 / n}$$

$$\sigma_{Z,y} = \sqrt{\sum_{i=1}^{n}\left(Z_y^i - \overline{Z}_y\right)^2 / n} \qquad (5.4)$$

$$\sigma_{Z,h} = \sqrt{\sum_{i=1}^{n}\left(Z_h^i - \overline{Z}_h\right)^2 / n}$$

here $\overline{Z}_j$ is the mean positioning error value for $j = x$, y and h, and n is the total number

of GPS outages.
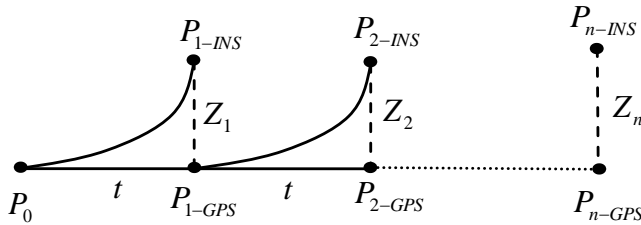
Figure 5.4. INS positioning errors (Zi) during GPS outages (t)

81

In Figure 5.4 P_0 is the initial position, $P_{i\text{-}INS}$ and $P_{i\text{-}GPS}$ are the positions estimated by INS

and GPS where $i=1:n$)

The positioning errors and the standard deviations of the scenarios defined in Chapter 5.3

are presented in Table 5.5 and Table 5.6 for HG1700 and HG1900, respectively.

Original	$\bar{Z}$ = 0.01618 m σ_Z = 0.27299 m							
Scenario	Solution Type		$t=1$ minute		$t=3$ minutes		$t=5$ minutes	
	Gyro	Accel.	$\bar{Z}$ (m)	σ_Z (m)	$\bar{Z}$ (m)	σ_Z (m)	$\bar{Z}$ (m)	σ_Z (m)
Scenario 1	3-par.	9-par.	0.01651	0.28071	0.01671	0.27206	0.01673	0.27218
	9-par.	9-par.	0.01520	0.24951	0.01607	0.23444	0.01589	0.23010
Scenario 2	3-par.	9-par.	0.01635	0.27577	0.01663	0.27121	0.01670	0.27098
	9-par.	9-par.	0.01585	0.24183	0.01615	0.28239	0.01629	0.24644
Scenario 3	3-par.	9-par.	0.01633	0.26955	0.01710	0.27249	0.01663	0.27226
	9-par.	9-par.	0.01595	0.24425	0.01572	0.24107	0.01642	0.26042
Scenario 4	3-par.	9-par.	0.01584	0.29263	0.01634	0.27848	0.01643	0.27798
	9-par.	9-par.	0.01520	0.22062	0.01532	0.22819	0.01532	0.22569

Table 5.5. Mean positioning errors and standard deviations of the defined scenarios for
HG1700

Here, t is the attitude data length (in minutes), $\bar{Z}$ is the mean position error and σ_Z is the

standard deviation of the position error (e.g. equation 5.3). The given values for the

Original case (Table 5.5) are obtained by using 0 (zeros) for the initial IMU error states

and the corresponding factory defined standard deviations (Table 2.1) in the EKF. In

addition, for the cases that the 3-parameter solution values were used in the initial states,

again the remaining scale factor error and non-orthogonality error values were set to 0 and their standard deviations were obtained from Table 2.1.

The standard deviation estimates of the position error showed that the most accurate results were obtained for Scenario 4 when the 9-parameter solution was used for the gyroscopes and for $t=1$ minute, which improved the estimation accuracy by 19%. However, the worst result was acquired again with Scenario 4 and the 3-parameter solution with $t=1$ minute, which decreased the accuracy by 7%. The estimates have shown that the 9-parameter solution performed better than the 3-parameter solution even though the scale factor error and non-orthogonality error estimates were quite large.

Original	$\overline{Z} = 0.00071$ m $\sigma_Z = 0.26772$ m							
Scenario	Solution Type		$t = 1$ minute		$t = 3$ minutes		$t = 5$ minutes	
	Gyro	Accel.	$\overline{Z}$ (m)	σ_Z (m)	$\overline{Z}$ (m)	σ_Z (m)	$\overline{Z}$ (m)	σ_Z (m)
Scenario 1	3-par.	9-par.	0.01817	0.25741	0.01817	0.25742	0.01817	0.25742
	9-par.	9-par.	0.01825	0.25670	0.01827	0.25648	0.01828	0.25644
Scenario 2	3-par.	9-par.	0.01815	0.25740	0.01815	0.25741	0.01816	0.25741
	9-par.	9-par.	0.01826	0.25652	0.01837	0.25620	0.01839	0.25620
Scenario 3	3-par.	9-par.	0.01817	0.25744	0.01818	0.25745	0.01816	0.25740
	9-par.	9-par.	0.01825	0.25692	0.01824	0.25691	0.01826	0.25666
Scenario 4	3-par.	9-par.	0.01821	0.25727	0.01821	0.25726	0.01823	0.25729
	9-par.	9-par.	21.72845	31.48215	0.01861	0.25578	0.01848	0.25734

Table 5.6. Mean positioning errors and standard deviations of the defined scenarios for HG1900

Except for Scenario 4, the positioning error estimations acquired were analogues for the HG1900. The results were very similar to each other within the cases when the 3-parameter solution and 9-parameter solution were used for gyroscope calibration. However, again the most and least accurate results were obtained in Scenario 4 for $t=2$ minutes (standard deviation increased by 4.5%) and $t=1$ minute, respectively. The EKF is very sensitive to the initial parameters included in the system. Therefore, because very large scale factor values were obtained in Scenario 4 for $t=1$ minute, the estimated positioning error and its standard deviation for this case was larger than the remaining estimations by about 31.2m. The cause of this exceptional situation is unknown. The following 2 figures demonstrates the standard deviations of the position estimations for 2s GPS signal outages for the HG1700 and HG1900.
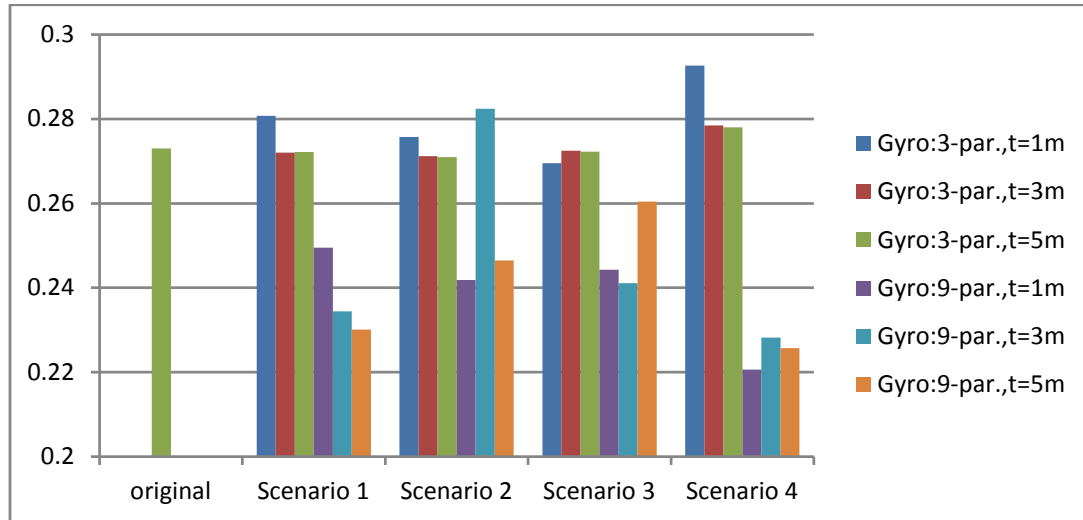
Figure 5.5. Positioning error standard deviations of the calibration scenarios for HG1700
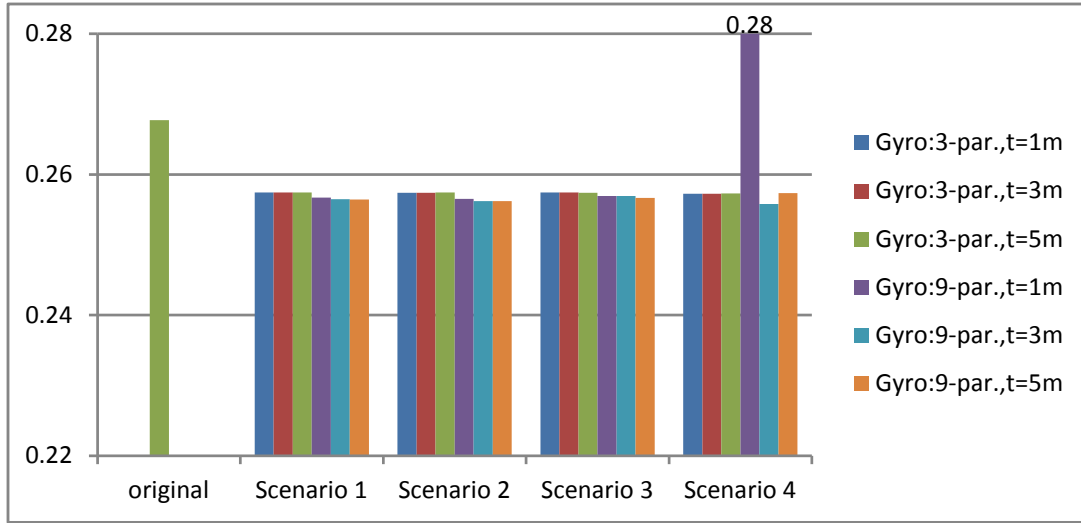
Figure 5.6. Positioning error standard deviations of the calibration scenarios for HG1900

By looking at the results above, it is not possible to decide which scenario must be used because there was no consistent increase or decrease in accuracies among the scenarios although each of them includes different amount and type of IMU attitude measurements. On the other hand, it can be concluded that Scenario 3, with 10 IMU attitude measurements, the 9-parameter solution and $t=3$minutes (3 minutes of data for each attitude) can be chosen as a decent solution. The results have already shown that using more attitude data with longer recording times do not improve the positioning accuracy significantly. Moreover, the 9-parameter solution mostly provided more accurate results than the 3-parameter solution although the scale factor error and non-orthogonality results are very large and unrealistic values.

Finally, in most of the cases, the HG1700 performs slightly better than the HG1900 when the 9-parameter solution was used (for the gyroscopes) while it is the opposite if the 3-

parameter solution was used. Even though the HG1700 is a slightly higher grade IMU than HG1900, HG1900 provided consistent improvement in estimating the position for both 3-parameter and 9-parameter solutions, where the latter provides more accurate results.

Different variations of Scenario 3 (with $t=3$ minutes) were also tested for longer GPS signal outages, and the results are presented in the table below. Meanwhile, the factory defined standard deviations were again used for the Original case while the error parameters were equal to 0, which can be considered as no calibration. In Scenario 3.0, it was aimed to test the accuracy of calibrating the IMU data only for the accelerometer errors. Therefore, the chosen gyroscope error parameters were equal to the Original case error parameters. Scenario 3.3 included the 3-parameter solution for the gyroscope error estimates while the 9-parameter solution for the gyroscope errors was used in Scenario 3.9. Moreover, for these 3 sub-scenarios, the accelerometer error estimates were obtained from the 9- parameter solution results of Scenario 3.

IMU	GPS gap	Parameter	Original	Scenario 3.0	Scenario 3.3	Scenario 3.9
HG1700	2s	$\bar{Z}$ (m)	0.0162	0.0167	0.0168	0.0157
		σ_Z (m)	0.2730	0.2723	0.2749	0.2411
	10s	$\bar{Z}$ (m)	0.1098	0.1318	0.1318	0.1673
		σ_Z (m)	2.9097	2.7409	2.7400	2.8066
	30s	$\bar{Z}$ (m)	1.8914	2.2924	2.2906	2.6714
		σ_Z (m)	16.2178	14.8938	14.8698	15.5484
	60s	$\bar{Z}$ (m)	26.7914	24.0717	23.9707	28.4346
		σ_Z (m)	183.4135	147.1561	147.8637	178.1520
HG1900	2s	$\bar{Z}$ (m)	0.0007	0.0182	0.0182	0.0182
		σ_Z (m)	0.2677	0.2572	0.2574	0.2569
	10s	$\bar{Z}$ (m)	0.1978	0.1989	0.1993	0.2439
		σ_Z (m)	6.7849	6.8077	6.8291	6.8420
	30s	$\bar{Z}$ (m)	2.1299	2.0695	2.0353	2.8572
		σ_Z (m)	21.2205	23.0985	23.1007	24.6951
	60s	$\bar{Z}$ (m)	17.9284	13.9221	13.7034	18.3633
		σ_Z (m)	92.3565	76.5114	75.9497	83.7324

Table 5.7. Mean position errors ($\bar{Z}$) and standard deviations (σ_Z) for different variations of Scenario 3 with t=3 minutes, (for HG1700 and HG1900)

For the HG1700, although the gyroscope estimates obtained by the 9-parameter solution (3.9) usually provided more accurate positioning results for 2s GPS outages, using 3-parameter solution gyroscope estimates (Scenario 3.3) or calibrating the data for only the accelerometer errors (Scenario 3.0) performed significantly better for the longer GPS outages. Moreover, the accuracy of Scenarios 3.3 were slightly better than Scenario 3.0 for 10s (by 0.03%) and 30s (by 0.15%) outages while Scenario 3.0 performed 0.39% better for the results of the 60s outage.

Similar to the HG1700, the HG1900 provided its most precise positioning estimates by Scenario 3.9 for 2s GPS outage. However, Scenario 3.3 yielded the best standard

deviation estimates for the 60s outage. In addition, for the 10s and 30s outages, calibrating with the factory given standard deviations (Original) produced the most precise estimates. Finally, HG1900 provided more accurate estimates for 10s and 30s GPS outages, while it was opposite for the remaining outages. The following 2 figures present the positioning error standard deviations of Scenario 3 with the defined sub-scenarios.
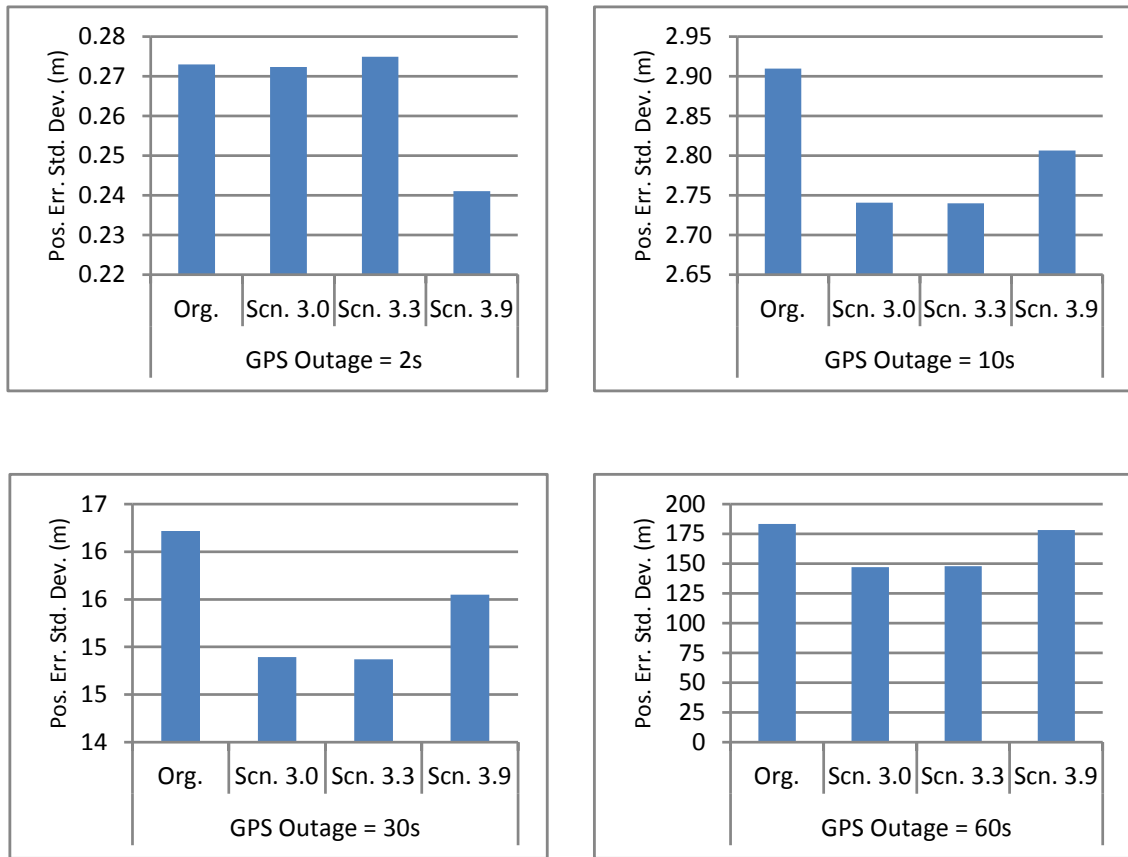
Figure 5.7. HG1700 Positioning error standard deviations of Scenario 3 with the defined sub-scenarios, due to the GPS outages
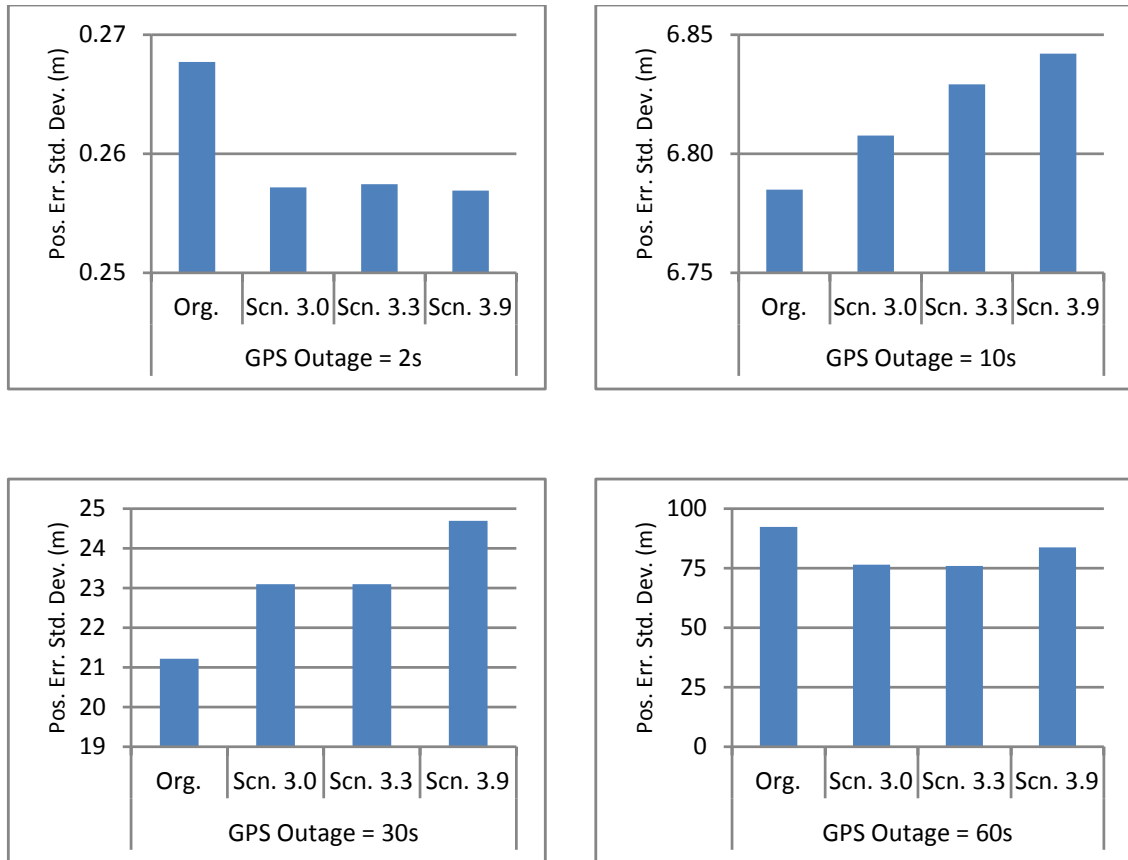
Figure 5.8. HG1900 Positioning error standard deviations of Scenario 3 with the defined sub-scenarios, due to the GPS outages

5.5 Summary

In this chapter, performance analyses of the Multi-Position Calibration Method were studied for the tactical grade IMUs, HG1700 and HG1900. The IMUs and a GPS receiver were installed on a cart together with the GPS antenna and the remaining instruments (see Figure 5.1). Then a field navigation test was conducted in the parking lot of OSU after performing relevant calibration measurements. The IMU error estimates showed that it is

possible to obtain good estimates for all 9 accelerometer errors. However, very large gyroscope scale factor error and non-orthogonality error values were obtained as expected based on the studies of Shin (2002) and Syed et al. (2007), and also the simulation study (Chapter 4.4.1). On the other hand, the positioning accuracy estimates showed that using the 9-parameter gyro error estimates, even though they were very large, provided more accurate results than the 3-parameter solution for both of the IMUs. For the 2s GPS outages, the HG1700 usually performed better than the HG1900 in terms of the positioning accuracies of calibrating the IMU data for the 9-parameter gyroscope solution error estimates. However, the HG1900 results were consistent, and thought to be more reliable. It has been experienced that using 10 IMU attitudes (Scenarios 3 and 4) and $t=3$minutes for each attitude should be enough because an increase in the used attitude numbers and the attitude data recording time did not provide a significant increase in positioning accuracies. Moreover, spending more time before starting the navigation mission is not desired unless it yields considerable improvement to the navigation estimations. Therefore, Scenario 3 was selected for the later tests where longer GPS outages were examined. Unlike the 2s outage estimates, the 9-parameter gyro estimates provided the worst positioning estimates for the longer GPS outages (10s, 30s and 60s). Therefore, it might be concluded that for short outages, using 9-parameter gyroscope error estimates can significantly contribute to the positioning accuracy while using the 3-parameter solution gyroscope estimates or calibrating the IMU data only for the accelerometer errors will provide more accurate results for longer outages for both of the IMUs.

90

Chapter 6: Conclusion

This study attempted to test the performance of the Multi-Position Calibration Method on the tactical grade IMUs. First, a simulation study was performed by the author by producing gyroscope and accelerometer data sets for all possible 26 IMU attitudes. The IMU errors were estimated by using the simulation data and the results were presented in Chapter 4. Then, in order to see the actual performance of the calibration method a cart based geolocation system was employed for this purpose and a field navigation test was conducted in the parking lot of OSU after collecting 26 IMU attitude data for the calibration estimations. The INS and GPS data were processed by an EKF developed in Lee (2009).

The simulation study has proven that all 9 accelerometer errors can be estimated with a nominal reference gravity value. 9 or more IMU attitude measurements will be enough for this. However, only the gyroscope bias can reasonably be obtained unless the reference rotation rate, the Earth rotation rate, is increased by about 10^4.

The field test has shown consistent results with both the simulation study and studies of Shin (2002) and Syed et al. (2007) in terms of IMU error estimations. The 9 accelerometer errors (biases, scale factor errors and non-orthogonality errors) and only gyroscope biases were reasonably estimated with the current reference signals. The remaining gyroscope error estimates were very large and unrealistic. Among the 2 tactical grade IMUs, the HG1700 usually performed better than the HG1900 as expected,

because of HG1700 being a slightly higher grade IMU. However, the HG1900 estimates were more consistent in estimating the IMU errors with an the increase in attitude numbers and attitude data lengths.

Based on the estimation accuracies, it can be concluded that 10 3-minute-long IMU measurements should be enough for the calibration purpose. Longer and more attitude measurements might improve the positioning accuracy, but the study has shown that it did not provide a significant contribution. However, use of non-orthogonality errors that are obtained from the previous calibration studies can decrease the required attitude number to 6 (if the same IMU is used) because these errors do not change with every turn-on and off of the IMUs.

The positioning accuracy estimates have shown that except for the 2s GPS outages, calibrating the IMU data for the estimated gyroscope errors did not improve the positioning accuracy significantly. For 2s outages, calibrating the IMU data with the 9-parameter solution gyroscope error estimates provided the most accurate positions. However, for longer GPS outages, it is not possible to decide on an optimum way to calibrate the IMU data. However, together with calibrating the IMU data for 9-parameter solution accelerometer errors, it was experienced that calibrating the IMU data with the 3-parameter solution gyroscope error estimates or the factory given gyroscope parameters provided more accurate results than calibrating the data using the 9-parameter solution gyroscope error estimates.

For accurate positioning with INS, the gyroscope scale factor and non-orthogonality errors must be determined precisely. For this purpose, a turntable can be used to increase

the reference rotation rate, e.g. the Modified Multi-Position Calibration Method (Syed et al., 2007), and one if the stochastic models, e.g Allan Variance (Aggarwal et al., 2008) and wavelet de-noising (Nassar and El-Sheimy, 2005) can be used.

References

Aggarwal, P., Syed, Z., Niu, X. and El-Sheimy, N. (2008), A Standard Testing and Calibration for Low Cost MEMS Inertial Sensors and Units, *Journal of Navigation*, 611, 323-336.

Artese, G. and Trecroci, A. (2008), Calibration of a Low Cost MEMS INS Sensor for an Integrated Navigation System, The International Archives of the Photogrammetry, *Remote Sensing and Spatial Information Sciences*. Vol. XXXVII. Part B5. Beijing.

Godha, S. (2006), Performance Evaluation of Low Cost MEMS-Based IMU Integrated with GPS for Land Vehicle Navigation Application, Thesis, UCGE reports Number 20239, The University of Calgary, Calgary, Alberta, Canada.

Goodall, C. L. (2009), Improving Usability of Low-Cost INS/GPS Navigation Systems Using Intelligent Techniques, Dissertation, UCGE reports Number 20276, The University of Calgary, Calgary, Alberta, Canada.

Honeywell Tactical Inertial Measurement Units (IMU) (2007), http://www51.honeywell.com/aero/common/documents/myaerospacecatalog-documents/Missiles-Munitions/Honeywell_Tactical_Inertial_Measurement_Units.pdf

Hou, H. (2004), Modeling Inertial Sensor Errors Using Allan Variance, Thesis, UCGE reports Number 20201, The University of Calgary, Calgary, Alberta, Canada.

Jekeli, C. (2000), Inertial Navigation Systems with Geodetic Applications, Walter de Gruyter, Inc., Berlin.

Jekeli, C. (2006), Geometric reference Systems in Geodesy, Lecture Notes, Division of Geodesy and Geospatial Sciences, School of Earth Sciences, Ohio State University, Columbus, Ohio, USA.

Jekeli, C. and Lee, J. K. (2007), Technical Assessment of IMU-Aided Geolocation Systems for UXO Detection and Characterization, Technical Report, the Ohio State University, Columbus, Ohio, USA.

Krakiwsky, E. J. (1978), A Synthesis of Recent Advances in the Method of Least Squares, Department of Surveying Engineering, University of New Brunswick, Fredericton, Canada.

94

Lee, J. K. (2009), The Estimation Methods for an Integrated INS/GPS UXO Geolocation System, Technical Report, the Ohio State University, Columbus, Ohio, USA.

May, N. C. (2008). A Rigorous Approach to Comprehensive Performance Analysis of State-of-the-Art Airborne Mobile Mapping Systems, Dissertation, The Ohio State University, Columbus, Ohio, USA.

Nassar, S. (2003), Improving the Inertial Navigation System (INS) Error Model for INS and INS/DGPS Applications, Dissertation, UCGE reports Number 20183, The University of Calgary, Calgary, Alberta, Canada.

Nassar, S. and El-Sheimy, N. (2005), Wavelet Analysis for Improving INS and INS/DGPS Navigation Accuracy, *the Journal of Navigation*, 58, 119–134.

Nassar, S. and El-Sheimy, N. (2006), A combined algorithm of improving INS error modeling and sensor measurements for accurate INS/GPS navigation, *GPS Solut*. 10: 29–39.

Nebot, E. and Durrant-Whyte, H. (1999), Initial Calibration and Alignment of Low-Cost Inertial Navigation Units for Land Vehicle Applications, *Journal of Robotic Systems*, 16(2), 81-92.

Perreault, J. M. A. (2008), Augmented Kalman Filter/Artificial Intelligence for Inertial Sensors/GPS Data Fusion, Thesis, the Royal Military College of Canada, Ottawa, ON, Canada.

Pope, A. J. (1972), Some Pitfalls to be avoided in the Iterative Adjustment of Nonlinear Problems, proceedings of the 38th Annual Meeting, American Society of Photogrammetry, Washington, D. C.

Salychev, O. (2004), Applied Inertial Navigation Solutions: Problems and Solutions, the BMSTU Press, Moscow, Russia.

Schaffrin, B. and Snow, K. (2009), Total Least-Squares Regularization of Tykhonov Type and an Ancient Racetrack in Corinth, *Linear Algebra Appl*., doi:10.1016/j.laa.2009.09.014.

Shin, E-H. (2001). Accuracy Improvement of Low Cost INS/GPS for Land Applications, Thesis, UCGE reports Number 20156, The University of Calgary, Calgary, Alberta, Canada.

Shin, E-H. and El-Sheimy, N. (2002), A New calibration Method for Strapdown Inertial Navigation Systems, *Z. Vermess*. 127 1-10.

Syed, Z. F. (2009), Design and Implementation Issues of a Portable Navigation System, Dissertation, UCGE reports Number 20288, The University of Calgary, Calgary, Albert, Canada.

Syed, Z.F., Aggarwal, P., Goodall, C., Niu, X. and El-Sheimy, N. (2007), A New Multi-Position Calibration Method for MEMS Inertial Navigation Systems, *Measurement Science and Technology*, 18, 1897-1907.

Weston, J.L., and Titterton, D. H. (2000), Modern Inertial Navigation Technology and Its Application, *Electronics & Communication Engineering Journal.*

Yi, Y. (2007), On Improving the Accuracy and Reliability of GPS/INS-Based Direct Sensor Georeferencing, Dissertation, The Ohio State University, Columbus, Ohio, USA.

Appendix A: Gyroscope Deterministic Error Estimations

Scenario 1: 26 attitudes			$t = 1$minute		$t = 3$minutes		$t = 5$minutes	
			Estimates	σ	Estimates	σ	Estimates	σ
Bias (rad/s)	HG1700	$b_{\omega x}$	6.00E-06	2.31E-06	3.57E-06	1.22E-06	4.61E-06	1.44E-06
		$b_{\omega y}$	-2.92E-06	2.30E-06	-1.75E-06	1.21E-06	-2.83E-06	1.42E-06
		$b_{\omega z}$	-3.34E-06	1.99E-06	1.12E-07	1.06E-06	1.23E-07	1.23E-06
	HG1900	$b_{\omega x}$	-3.05E-06	1.77E-06	-3.02E-06	2.29E-06	-2.15E-06	2.47E-06
		$b_{\omega y}$	1.29E-05	1.80E-06	1.38E-05	2.32E-06	1.27E-05	2.52E-06
		$b_{\omega z}$	1.32E-05	1.61E-06	1.38E-05	2.05E-06	1.39E-05	2.19E-06

Table A.1. 3-parameter solution gyroscope error estimates of the HG1700 and HG1900 for Scenario 1

Scenario 1: 26 attitudes			$t = 1$minute		$t = 3$minutes		$t = 5$minutes	
			Estimates	σ	Estimates	σ	Estimates	σ
HG1700	Bias (rad/s)	$b_{\omega x}$	3.12E-06	3.46E-06	2.68E-06	1.72E-06	3.30E-06	2.09E-06
		$b_{\omega y}$	-1.19E-06	2.25E-06	-1.09E-06	1.55E-06	-1.73E-06	1.85E-06
		$b_{\omega z}$	-2.53E-06	2.52E-06	-7.36E-08	1.34E-06	1.68E-07	1.54E-06
	Scale Fac. (ppm)	$s_{\omega x}$	151588.13	91281.72	31234.80	40250.16	46403.94	50490.55
		$s_{\omega y}$	-70816.33	49915.25	-11340.98	33990.76	-4641.01	40368.77
		$s_{\omega z}$	73639.86	51540.41	20757.98	27410.23	6861.07	30942.31
	Non-orth. (μrad)	$\theta_{\omega yz}$	68800.65	70441.37	15443.10	43445.64	31594.46	51605.53
		$\theta_{\omega zx}$	-8153.25	56304.02	17357.42	35618.85	20540.38	41958.56
		$\theta_{\omega zy}$	-137854.18	70499.00	-792.32	38491.11	3300.88	45584.23
HG1900	Bias (rad/s)	$b_{\omega x}$	-3.81E-06	2.06E-06	-3.61E-06	2.46E-06	-3.06E-06	2.81E-06
		$b_{\omega y}$	1.33E-05	2.18E-06	1.40E-05	2.60E-06	1.32E-05	2.87E-06
		$b_{\omega z}$	1.26E-05	1.82E-06	1.27E-05	2.38E-06	1.29E-05	2.59E-06
	Scale Fac. (ppm)	$s_{\omega x}$	-384.12	47872.79	-26071.13	55029.64	-14575.18	63693.76
		$s_{\omega y}$	26674.33	50595.14	1418.93	58634.18	-6911.75	63725.03
		$s_{\omega z}$	17018.44	35945.82	72046.34	47388.70	67565.05	51617.42
	Non-orth. (μrad)	$\theta_{\omega yz}$	20956.14	56084.43	40622.36	69566.33	55085.88	77418.75
		$\theta_{\omega zx}$	-14237.39	56418.50	-21227.53	68211.42	-3340.57	75021.34
		$\theta_{\omega zy}$	64462.97	58938.76	78134.27	70602.18	73005.73	77451.32

Table A.2. 9-parameter solution gyroscope error estimates of the HG1700 and HG1900 for Scenario 1

Scenario 2: 18 attitudes			$t = 1$ minute		$t = 3$ minutes		$t = 5$ minutes	
			Estimates	σ	Estimates	σ	Estimates	σ
Bias (rad/s)	HG1700	$b_{\omega x}$	1.84E-06	1.17E-06	2.57E-06	1.61E-06	2.26E-06	1.47E-06
		$b_{\omega y}$	-3.18E-07	1.13E-06	-8.77E-07	1.52E-06	-1.34E-06	1.39E-06
		$b_{\omega z}$	-4.40E-07	9.98E-07	1.08E-06	1.34E-06	1.27E-06	1.22E-06
	HG1900	$b_{\omega x}$	-2.45E-06	2.18E-06	-2.50E-06	3.29E-06	-3.25E-06	3.38E-06
		$b_{\omega y}$	1.24E-05	2.12E-06	1.27E-05	3.20E-06	1.16E-05	3.32E-06
		$b_{\omega z}$	1.27E-05	1.85E-06	1.36E-05	2.75E-06	1.32E-05	2.82E-06

Table A.3. 3-parameter solution gyroscope error estimates of the HG1700 and HG1900 for Scenario 2

Scenario 2: 18 attitudes			$t = 1$ minute		$t = 3$ minutes		$t = 5$ minutes	
			Estimates	σ	Estimates	σ	Estimates	σ
HG1700	Bias (rad/s)	$b_{\omega x}$	1.06E-07	8.27E-07	2.30E-06	1.88E-06	1.89E-06	1.72E-06
		$b_{\omega y}$	9.61E-07	8.41E-07	-1.38E-06	1.89E-06	-1.76E-06	1.73E-06
		$b_{\omega z}$	-1.19E-06	6.87E-07	-3.59E-07	1.90E-06	-7.81E-08	1.68E-06
	Scale Fac. (ppm)	$s_{\omega x}$	23415.90	22729.18	-7434.72	53418.82	-4120.09	49308.02
		$s_{\omega y}$	7805.72	18576.47	-11017.17	43563.63	-5427.93	39757.47
		$s_{\omega z}$	20795.70	15198.69	61875.68	41646.15	51582.20	36439.91
	Non-orth. (µrad)	$\theta_{\omega yz}$	74107.57	21208.71	-10315.82	51206.11	-10278.80	46451.98
		$\theta_{\omega zx}$	14318.25	20389.63	-17065.05	49389.85	-12987.98	44385.99
		$\theta_{\omega zy}$	55057.72	20085.33	19985.82	53008.66	27751.40	47537.60
HG1900	Bias (rad/s)	$b_{\omega x}$	-3.39E-06	1.89E-06	-3.60E-06	2.40E-06	-4.02E-06	2.40E-06
		$b_{\omega y}$	1.08E-05	3.11E-06	9.86E-06	4.54E-06	7.99E-06	4.90E-06
		$b_{\omega z}$	1.10E-05	2.32E-06	9.61E-06	4.10E-06	8.15E-06	4.54E-06
	Scale Fac. (ppm)	$s_{\omega x}$	-86310.47	50540.68	-115397.89	60573.89	-122281.04	59480.34
		$s_{\omega y}$	114603.73	70625.94	109225.84	98015.48	113521.00	100261.79
		$s_{\omega z}$	47965.72	48440.72	168799.40	89136.59	184656.04	96069.95
	Non-orth. (µrad)	$\theta_{\omega yz}$	48423.30	62283.94	60290.58	84801.68	48178.77	87013.46
		$\theta_{\omega zx}$	-80403.75	79787.83	-156284.05	119476.68	-157727.12	124127.98
		$\theta_{\omega zy}$	91407.23	65398.04	135732.86	85133.61	142035.43	84410.47

Table A.4. 9-parameter solution gyroscope error estimates of the HG1700 and HG1900 for Scenario 2

Scenario 4: Last 10 attitudes			$t = 1$minute		$t = 3$minutes		$t = 5$minutes	
			Estimates	σ	Estimates	σ	Estimates	σ
Bias (rad/s)	HG1700	$b_{\omega x}$	1.38E-05	4.43E-06	5.79E-06	1.37E-06	9.02E-06	2.04E-06
		$b_{\omega y}$	-7.10E-06	4.74E-06	-2.44E-06	1.45E-06	-5.13E-06	2.10E-06
		$b_{\omega z}$	-8.82E-06	4.05E-06	-2.03E-06	1.33E-06	-2.43E-06	1.90E-06
	HG1900	$b_{\omega x}$	-3.84E-06	3.08E-06	-3.27E-06	2.46E-06	-6.82E-07	3.20E-06
		$b_{\omega y}$	1.35E-05	3.22E-06	1.59E-05	2.49E-06	1.37E-05	3.22E-06
		$b_{\omega z}$	1.45E-05	3.35E-06	1.39E-05	2.64E-06	1.49E-05	3.31E-06

Table A.5. 3-parameter solution gyroscope error estimates of the HG1700 and HG1900 for Scenario 4

Scenario 4:			$t = 1$minute		$t = 3$minutes		$t = 5$minutes	
			Estimates	σ	Estimates	σ	Estimates	σ
HG1700	Bias (rad/s)	$b_{\omega x}$	7.38E-06	4.18E-06	3.06E-06	4.08E-06	6.75E-06	2.87E-06
		$b_{\omega y}$	-7.14E-07	1.77E-06	-6.15E-07	3.54E-06	-4.19E-06	2.37E-06
		$b_{\omega z}$	-7.03E-06	3.49E-06	-3.01E-07	1.92E-06	1.79E-07	1.27E-06
	Scale Fac. (ppm)	$s_{\omega x}$	285657.03	67602.11	63714.45	54836.11	77802.06	40670.06
		$s_{\omega y}$	-55141.78	28561.37	56469.02	65158.08	68806.32	46977.00
		$s_{\omega z}$	275992.08	78622.51	-65465.49	35556.50	-97401.07	21956.00
	Non-orth. (μrad)	$\theta_{\omega yz}$	-15374.04	78801.22	86162.59	101247.38	99520.37	73642.71
		$\theta_{\omega zx}$	116969.27	62626.11	-57254.64	75559.38	-123230.17	52949.37
		$\theta_{\omega zy}$	-402928.76	58031.96	16494.06	52393.64	28553.97	40699.47
HG1900	Bias (rad/s)	$b_{\omega x}$	-1.57E-04	8.02E-04	-5.50E-06	6.74E-06	-2.67E-05	3.96E-05
		$b_{\omega y}$	1.96E-04	1.05E-03	1.64E-05	4.33E-06	4.10E-05	5.81E-05
		$b_{\omega z}$	2.47E-05	4.87E-05	1.63E-05	2.60E-06	2.16E-05	7.73E-06
	Scale Fac. (ppm)	$s_{\omega x}$	2215121.62	11094977.31	117577.47	66593.74	424854.38	553295.22
		$s_{\omega y}$	2770940.05	14880905.66	-11655.24	142047.34	-2641188.00	1172345.78
		$s_{\omega z}$	199300.14	1795454.44	-104920.61	57383.11	-116854.00	112351.40
	Non-orth. (μrad)	$\theta_{\omega yz}$	889215.64	1513656.26	-7812.47	151703.57	-415399.79	491399.71
		$\theta_{\omega zx}$	-527971.07	455632.16	-158267.36	165087.87	504809.13	321445.72
		$\theta_{\omega zy}$	130048.59	852101.72	238484.16	121549.01	263015.51	214255.04

Table A.6. 9-parameter solution gyroscope error estimates of the HG1700 and HG1900 for Scenario 4

Appendix B: Accelerometer Deterministic Error Estimations

9-Parameter Solution			$t = 1\text{minute}$		$t = 3\text{minutes}$		$t = 5\text{minutes}$	
			Estimates	σ	Estimates	σ	Estimates	σ
HG1700	Bias (m/s^2)	b_{gx}	3.91E-03	5.74E-04	4.24E-03	1.94E-04	4.32E-03	1.76E-04
		b_{gy}	-1.04E-03	5.40E-04	-1.06E-03	1.82E-04	-1.19E-03	1.66E-04
		b_{gz}	3.53E-03	5.26E-04	3.62E-03	1.77E-04	3.53E-03	1.61E-04
	Scale Fac. (ppm)	s_{gx}	-176.26	78.58	-157.09	26.52	-138.70	24.14
		s_{gy}	178.32	78.49	171.04	26.49	156.57	24.11
		s_{gz}	75.02	77.47	70.80	26.15	73.18	23.80
	Non-orth. (μrad)	θ_{gyz}	214.04	131.05	11.75	44.24	-35.96	40.26
		θ_{gzx}	107.77	112.40	90.42	37.94	92.65	34.53
		θ_{gzy}	157.09	121.20	74.72	40.91	37.72	37.23
HG1900	Bias (m/s^2)	b_{gx}	-3.29E-03	4.05E-04	-3.36E-03	3.52E-04	-3.36E-03	3.57E-04
		b_{gy}	-4.56E-03	3.82E-04	-4.41E-03	3.32E-04	-4.26E-03	3.37E-04
		b_{gz}	1.75E-03	3.71E-04	1.85E-03	3.22E-04	1.93E-03	3.27E-04
	Scale Fac. (ppm)	s_{gx}	56.30	55.47	51.33	48.20	44.90	48.98
		s_{gy}	89.91	55.61	92.93	48.33	86.00	49.09
		s_{gz}	166.81	54.78	157.71	47.61	150.39	48.36
	Non-orth. (μrad)	θ_{gyz}	-40.26	92.60	-17.56	80.48	-1.67	81.76
		θ_{gzx}	-146.52	79.55	-127.73	69.13	-103.48	70.23
		θ_{gzy}	-124.25	85.51	-122.92	74.31	-130.49	75.50

Table B.1. 9-parameter solution accelerometer error estimates of the HG1700 and HG1900 for Scenario 1

9-Parameter Solution			$t = 1$minute		$t = 3$minutes		$t = 5$minutes	
			Estimates	σ	Estimates	σ	Estimates	σ
HG1700	Bias (m/s²)	b_{gx}	4.18E-03	9.42E-04	4.58E-03	2.97E-04	4.69E-03	2.31E-04
		b_{gy}	-1.14E-03	7.89E-04	-1.17E-03	2.49E-04	-1.33E-03	1.93E-04
		b_{gz}	3.58E-03	8.10E-04	3.67E-03	2.55E-04	3.60E-03	1.98E-04
	Scale Fac. (ppm)	s_{gx}	-197.11	113.37	-155.82	35.76	-125.88	27.77
		s_{gy}	185.81	101.99	179.52	32.17	172.51	24.97
		s_{gz}	59.22	102.62	55.80	32.38	60.22	25.14
	Non-orth. (μrad)	θ_{gyz}	355.03	227.34	75.49	71.71	54.37	55.68
		θ_{gzx}	91.83	182.72	79.15	57.65	107.80	44.76
		θ_{gzy}	180.61	212.31	48.36	66.97	3.82	52.00
HG1900	Bias (m/s²)	b_{gx}	-3.89E-03	3.89E-04	-3.89E-03	3.49E-04	-3.93E-03	3.36E-04
		b_{gy}	-4.55E-03	3.27E-04	-4.34E-03	2.94E-04	-4.13E-03	2.82E-04
		b_{gz}	1.76E-03	3.34E-04	1.91E-03	3.00E-04	2.03E-03	2.88E-04
	Scale Fac. (ppm)	s_{gx}	-36.94	46.79	-28.10	42.02	-39.79	40.41
		s_{gy}	87.78	42.28	91.44	37.96	80.72	36.50
		s_{gz}	205.83	42.39	188.17	38.06	178.35	36.60
	Non-orth. (μrad)	θ_{gyz}	-82.48	93.94	-37.16	84.36	-29.56	81.12
		θ_{gzx}	-181.64	75.71	-142.20	67.99	-103.90	65.38
		θ_{gzy}	-70.61	87.73	-80.17	78.77	-87.29	75.74

Table B.2. 9-parameter solution accelerometer error estimates of the HG1700 and HG1900 for Scenario 2

9-Parameter Solution			t = 1minute		t = 3minutes		t = 5minutes	
			Estimates	σ	Estimates	σ	Estimates	σ
HG1700	Bias (m/s²)	b_{gx}	3.04E-03	8.87E-04	3.67E-03	2.35E-04	3.86E-03	1.06E-04
		b_{gy}	-2.35E-03	1.92E-03	-1.19E-03	5.08E-04	-9.28E-04	2.29E-04
		b_{gz}	3.79E-03	9.20E-04	3.66E-03	2.44E-04	3.44E-03	1.10E-04
	Scale Fac. (ppm)	s_{gx}	-11.88	141.37	-105.86	37.47	-117.67	16.92
		s_{gy}	799.12	945.39	181.55	250.14	5.12	112.73
		s_{gz}	-544.67	870.58	30.37	231.17	180.53	104.27
	Non-orth. (µrad)	θ_{gyz}	9.13	161.61	-28.49	42.81	-85.67	19.34
		θ_{gzx}	207.65	151.20	97.74	40.08	54.37	18.09
		θ_{gzy}	79.35	157.18	72.96	41.70	40.18	18.84
HG1900	Bias (m/s²)	b_{gx}	-3.18E-03	2.12E-04	-3.28E-03	2.06E-04	-3.26E-03	1.73E-04
		b_{gy}	-4.74E-03	4.58E-04	-4.93E-03	4.47E-04	-5.05E-03	3.74E-04
		b_{gz}	1.72E-03	2.08E-04	1.85E-03	2.02E-04	1.95E-03	1.69E-04
	Scale Fac. (ppm)	s_{gx}	345.34	33.76	300.83	32.88	298.00	27.57
		s_{gy}	315.80	224.16	398.97	218.35	506.46	183.01
		s_{gz}	-230.29	207.86	-281.68	202.37	-377.32	169.51
	Non-orth. (µrad)	θ_{gyz}	-135.31	38.71	-124.02	37.70	-118.22	31.62
		θ_{gzx}	-58.01	29.56	-71.33	28.78	-61.18	24.12
		θ_{gzy}	-160.75	37.03	-144.87	36.05	-146.69	30.23

Table B.3. 9-parameter solution accelerometer error estimates of the HG1700 and HG1900 for Scenario 4